EFFECT OF INCIDENT LIGHT INTENSITY AND SOURCE – DETECTOR SEPARATION ON PHOTON MIGRATION DEPTH IN TURBID MEDIA

by

BETÜL ŞAHİN

B.S., Physics, METU, 2002

Submitted to the Institute of Biomedical Engineering
in partial fulfillment of the requirements
for the degree of
Master of Science
in
Biomedical Engineering

Boğaziçi University
June 2006

ACKNOWLEDGMENTS

I would like to thank to my supervisor Assist. Prof. Ata Akın for giving me the opportunity to work on this research topic which was an exciting and challenging experience in all aspects, his motivating approach and kind academic support.

I would like to thank Prof. Dr. İnci Çilesiz for being a member of my thesis committee.

I would like to thank Assist. Prof. Dr. Murat Gülsoy for being a member of my thesis committee.

This study is a part of BURF 04X1020 and DPT 03K120250 Boğaziçi University research project. I am grateful to Boğaziçi University for their support.

It was a pleasure to share the knowledge; I would like to thank valuable research assistants and staff off Biomedical Engineering Institute for their support.

Hasan and Meryem Şahin, this study is dedicated to you, thank you…

ABSTRACT

EFFECT OF INCIDENT LIGHT INTENSITY AND SOURCE – DETECTOR SEPARATION ON PHOTON MIGRATION DEPTH IN TURBID MEDIA

Diffuse optical tomography (DOT) and near-infrared spectroscopy (NIRS) are techniques that suffer from an uncertainty of photon migration pathlength which is important for information of the tissue depth that is probed. We have investigated the hypothesis that probing depth is a function of the incident light power and source-detector distance. The hypothesis is tested both numerically by Photon Migration Imaging (PMI) Toolbox (finite-element model diffusion approximation to the radiative transfer equation) and experimentally using continuous wave coherent light. Increasing the light power simultaneously increases the measured photon fluence, more importantly its effects on distribution of photon density can be seen by forming perturbations in the media. Simulations and experiments showed that it is possible to detect the presence of a layer with a higher absorption coefficient than the upper layer and its depth using the fact that different source – detector pairs' diffuse photons have different depths of most probable path of migration. We also showed that a change in the photon distribution with increasing intensity of incident light has no virtual contribution to this derivation.

Keywords: *Light propagation in tissue, diffuse optical tomography, photon migration and probe geometry.*

ÖZET

BULANIK ORTAMDA GİREN IŞIK GÜCÜ VE KAYNAK – ALICI MESAFESİNİN FOTON GÖÇÜ DERİNLİĞİNE ETKİLERİ

Işığın doku içinde yayılımını kullanan tıbbi görüntüleme tekniklerinin (DOT, NIRS) önemli sorunlarından biri ışığın aldığı yolun ve ne kadar derine indiğinin tam olarak bilinememesidir. Biz burada daha derinlerden bilgi almanın ışığın gücü ve alıcı kaynak mesafesi ile ilgili olduğu hipotezini araştırdık. Hipotez, PMI Toolbox (foton difüzyon yaklaşımını sonlu – elemanlar yöntemiyle çözen algoritmalar bütünü) yardımıyla sayısal olarak ve deneysel olarak test edildi. Giren ışık gücünü arttırmak doğrusal olarak alınan ışığı artırır, daha önemlisi bunun foton yoğunluğunun dağılımına etkileri ortamın derinliği azaltılarak görülebilir. Simülasyonlar ve deneyler gösterdi ki yarı – uzay geometride farklı mesafedeki alıcı kaynak çiftlerinin dağılan fotonlarının farklı, muhtemel göç yolu derinliği olması prensibi kullanılarak, üstteki katmandan daha yüksek soğurma özelliklerine sahip bir katmanı fark etmek ve derinliğini belirlemek mümkün. Ayrıca gösterildi ki giren ışığın gücü artırılarak gerçekleştirilen foton yoğunluğu dağılımındaki değişimin bu çıkarıma görünen bir katkısı yoktur.

Anahtar sözcükler: *Işığın dokuda yayılımı, dağılma optik tomografi, foton göçü, prob geometrisi*

TABLE OF CONTENTS

LIST OF FIGURES

LIST OF TABLES

LIST OF SYMBOLS

A	Attenuation
d	Optical pathlength
Io	Incident light intensity
I	Transmitted light intensity
μ_s	Scattering coefficient
g	Anisotropy factor
μ_s'	Reduced scattering coefficient
μ_a	Absorption coefficient
λ	Wavelength of radiation
$L(\mathbf{r}, \hat{\mathbf{s}}, t)$	Radiance
ν	Speed of electromagnetic wave in the medium
$\hat{\boldsymbol{s}}$	Unit direction vector
$p(\hat{\boldsymbol{s}}, \hat{\boldsymbol{s}}')$	Scattering phase function
$\hat{\Omega}$	Unit solid angle
μ_t	Optical transport coefficient
$\Phi(\mathbf{r}, t)$	Photon fluence rate
D	Diffusion coefficient
L_a	Diffusive absorption distance
κ	Inverse diffusive absorption distance
E	Electrical field
ε_o	Permittivity constant for vacuum

LIST OF ABBREVIATIONS

LASER	Light Amplification by the Stimulated Emission of Radiation
NIRS	Near Infrared Spectroscopy
DOT	Diffuse Optical Tomography
RTE	Radiative Transfer Equation
DPF	Differential Pathlenght Factor
CW	Continuous Wave
PDF	Photon Distribution Function
RF	Radio Frequency
PMI	Photon Migration Imaging
LDC	Laser Diode Controller
SD	Source – Detector
UPS	Uninterruptible Power Supply
LED	Light Emitting Diode

1. INTRODUCTION

1.1 Objective

The use of near-infrared spectroscopy (NIRS) to determine, non-invasively, the oxygenation of cerebral blood and tissue was first shown by Jöbsis (1977) in the cat [1]. The technique has since been developed to monitor cerebral oxygenation in the human adult (*1992*) and infant (1986). There is now considerable interest in the development of NIRS imaging of oxygenation distribution in intact organs and using light as an imaging tool; diffuse optical tomography (DOT) [2].

Everyday, we are exposed to light and it becomes diffuse in few millimetres of tissue. Diffuse photons, which have travelled centimetres of depth of tissue, can be detected with sensitive instrumentation. Light offers a safe and non-invasive means of monitoring biochemical, physiological and patophysiological changes of tissue, due to scattering and absorption properties.

Diffuse photons are not like x-ray radiation; they lack the information of position because they are scattered may times. We can consider a distribution of photon density, or mean photon path that reach the detector. In order to quantify data and hence determine chromophore concentrations, it is necessary to know the pathlength travelled by the light through the tissues. This pathlength can be determined from measurements of the time of flight of ultrashort pulses of light through the head, or derived from a measurement of the phase shift of frequency modulated light. Imaging with diffuse photons is a complicated process and acquires modelling of light propagation in tissue with a physical model to predict the chromophore positions or concentrations.

Diffuse photons' distribution in a semi-infinite geometry is similar to shape of a "banana" and their mean pathlength is a function of source detector separation and optical properties of the medium. Here we are concerned with the effect of incident light intensity on the distribution of diffuse photons. To investigate if incident light intensity can be used as another dimension for imaging, we designed a turbid medium in a semi – infinite geometry; ran computer simulations and performed experiments of near-infrared light (850

nm) propagation in turbid media. Simulations and experiments involved disturbing the banana pattern of diffuse photon density with perturbations and changing the intensity of light to see if there is a significant difference of diffuse photon density with changing intensity.

1.2 Outline

Following introduction, chapter two gives background of physical models of interaction of light and matter, tissue optical properties and DOT.

In chapter three we will introduce our methods of modeling and experimentation.

In chapter four we will present our results and discuss. In chapter five we will discuss the results and conclude in chapter six.

In addition; important information that was necessary for this research to proceed (data sheets of elements of experimental set-up etc.) that will hopefully be helpful for the reader to understand is given in the appendices.

2. THEORY

In order to understand how images can be generated from diffusely scattered light, one must first understand how light propagates through scattering media.

2.1 Interaction of Light and Matter

2.1.1 Optical Scattering

When a light source is placed in contact with the scalp, skin layer reflects about 5-7% of the incident light. Collimated light beam is transformed to diffuse one [3]. Scattering continues at each layer of the tissue due to unpredictable variation in refractive index at a microscopic and macroscopic scale such as membrane boundaries of cells, various organelles inside the cell because of the index mismatching between intra and extra cellular fluid. Cellular organelles such as mitochondria are thought to be the main scatterers in various tissues. Also Rayleigh scattering occurs at molecules that have smaller dimensions than the photons wavelength. Fraction of light that reach the detector is as little as 1 in 10^{-10} [4].

Among optical interactions; refraction is the deviation of a transmitted light ray upon crossing between two media that have different real indices of refraction. Refraction occurs at every optical interface, and is the dominant source of scattering in materials with a small relative index mismatch or a low scatterer concentration, like tissue, milk, and fog. Reflection is similar to refraction, but it refers to the portion of light that is directed away from the interface. Reflection is a symmetric process: the angle of incidence is identical to the angle of reflection. As a result of refractive index differences of the tissue (~1.34) and the air (~1.00), a fraction of the radiation coming from inside the tissue is reflected back into the turbid medium. Scattering in this context refers to any refraction or reflection that occurs either at an unpredictable location or deviates in an unpredictable direction. It can be thought of as “angular noise” in the light path of an optical system [4].

Optical scattering can be elastic or inelastic. Elastic scattering is the dominant scattering mechanism in diffuse imaging. It is caused by spatially abrupt (shorter than λ) changes in refractive index. The term “elastic” refers to the fact that the photon energy is

preserved – the scattered photons are at the same wavelength as they were prior to the scattering event. The average angular deviation of elastic scattering is a function of the particle size, shape, and index difference. Elastic scattering is the mechanism responsible for optical microscopy, as well as DOT.Inelastic scattering, of which fluorescence is a special form, always involves a change in the photon energy, and hence wavelength.

The attenuation (A) due to single scattering is proportional to the number density of the scattering particles (N), the scattering cross section of the particles (σs) and the optical pathlength (d):

$$A = \log_{10} [I_o / I] = N.\sigma_s.d \qquad (2.1)$$

I is the light intensity transmitted through the medium. The product Nσs is known as the scattering coefficient of the medium (μs), the reciprocal is the mean free path between scattering events. The scattering coefficients of human tissues are generally within the range 10 - 100 mm^{-1}, roughly one hundred times greater than those for absorption [5].

In biological tissues, scattering occurs principally in a forward direction, corresponding to an anisotropy in the range $0.69 > g > 0.99$**.** g which is mean cosine of the scattering angle, is called the *anisotropy factor*. Despite the forward scatter, typical values of scattering coefficient ensure that light travelling through more than a few millimeters of tissue loses all of its original directionality, and can be treated as effectively isotropically distributed. Thus it is convenient to express the characteristic scatter of tissues in terms of a *reduced scattering coefficient*:

$$\mu_s' = \mu_s (1 - g) \qquad (2.2)$$

which represents the effective number of isotropic scatters per unit length, and is a fundamental parameter in *diffusion theory.*

Due to highly forward scattering properties of tissue, visible and NIR light easily penetrates bone (g = 0.93). The most highly scattering tissues include bone, cerebral white matter, and skin dermis.

2.1.2 Optical Absorption

Absorption, in optics, is the process by which the energy of a photon is taken up by another entity. Absorbed light can be converted to heat or reradiated in the form of florescence or consumed in photo biochemical reactions. Beer-Lambert law relates the absorption of light to the properties of the material through which the light is travelling:

$$\ln [I_o / I] = \sigma_a.\rho.d \quad (2.3)$$

$$\text{or } A = \log_{10} [I_o / I] = a.c.d, \quad (2.4)$$

where, I_o is the incident intensity, I is the transmitted light intensity, σ_a is the absorption cross section, ρ is the number density of absorbing molecules, a is the specific extinction coefficient for a solution ($molar^{-1}cm^{-1}$), c is the concentration of absorbing molecules (mM), d is the pathlength (cm). The product 'ac' or '$\sigma_a\rho$' is known as absorption coefficient of the medium, μa. In a medium containing several different absorbing compounds:

$$A = \log_{10} [I_o / I] = [a_1.c_1 + a_2.c_2 + a_3.c_3 + ... + a_n.c_n]. d \quad (2.5)$$

Eq. 2.4 is used for spectroscopy; Eq. 2.3 is a relation for general optics. Due to its simplicity, the Beer-Lambert law is accurate only if the following conditions are met:

- The absorbing medium must be homogeneous
- The light source must be monochromatic
- Scattering and reflection must not occur

The effect of scattering is to substantially increase the path length travelled by photons and probability of absorption occurring. To address the scattering, the Beer-Lambert relationship must be modified to include (i) an additive term, *G*, due to scattering losses and (ii) a multiplier, differential pathlength factor (DPF), to account for the increased optical pathlength due to scattering:

$$A = \log_{10} [Io / I] = a.c.d.\ DPF + G \quad (2.6)$$

G is unknown and is dependent upon the measurement geometry and the scattering coefficient of the tissue interrogated. Therefore this equation provides a measure of the *absolute* concentration of the chromophore in the medium from a measure of *absolute* attenuation. However if *G* does not change during the measurement period, it is possible to determine a *change* in concentration (c_2-c_1) of the chromophore from a measured *change* in attenuation (A_2-A_1):

$$(A_2\text{-}A_1) = (c_2\text{-}c_1).a.d.\ \text{DPF} \tag{2.7}$$

The quantification of the change in concentration still depends upon the measurement of the geometrical distance *d* and the differential pathlength factor, i.e. the true optical pathlength which the scattered light has traveled. *d* is simple enough to measure, as it is purely the geometrical distance between the points where the light enters and leaves the medium and DPF is measured empirically.

2.1.3 Categories of Light Propagation

Ballistic light or transport means photons travel along straight lines or scatter at predictable locations preserving the image (Figure 2.1). In relatively transparent materials such as corneal tissue or cerebrospinal fluid, μ_a greatly exceeds μ_s, and light travels ballistically. Mirrors and lenses are designed using ballistic photon transport models. Our binocular vision relies upon ballistic photon transport.

Singly and 'fewly' scattered, 'snake' light paths are uncertain, and is difficult to characterize. Snake light is often encountered in ballistic imaging, where it reduces image contrast.

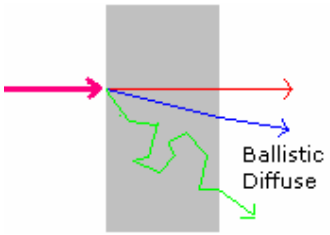

Figure 2.1 Ballistic and diffuse photon transport; light can either pass beyond directly or being multiply scattered follow complicated paths before exiting the medium.

Multiply scattered light is easier to model than snake light, and is best treated statistically, using either the diffusion equation or Monte Carlo simulations – much like heat flow or neutron flux (Figure 2.1).

2.2 Modeling Light Propagation in Diffuse Media

Reflection, refraction, and diffraction are all descriptions for different macroscopic effects of light-matter interactions. In a general sense, all of these involve elastic optical scattering. What differs is the nature and form of the scatterers. If the scatterer is macroscopic (in relation to a photon) and fixed in dimension and composition, then the "boundary" concepts of reflection and refraction and the " wave" concept of diffraction can be applied.

2.2.1 Single Particle Scattering Models

Rayleigh scattering and Mie models are two most commonly used models. According to Rayleigh formula for particle diameters much smaller than λ, the scattered intensity I_s is:

$$I_s \alpha \frac{V^2}{r^2 \lambda^4} \tag{2.8}$$

where; V is the particle volume, r is the distance of the particle from the point of observation and λ is the wavelength of the radiation.

Shorter wavelengths experience significantly greater scattering in the Rayleigh regime due to λ^4 effect (Eq. 2.8). Gas molecules are far smaller than 0.5 μm, and so act as Rayleigh scatterers, the sky appears blue, and not white or yellow. Clouds, however, are formed from water droplets or ice crystals that are typically far larger than 1 μm, and so act as Mie scatterers. This is why clouds appear white [4].

Mie scattering is based upon the assumption that the scattering particles are spherical. Although this is an ideal model for water droplets in air (i.e. clouds), it is less applicable to tissue, due to the wide variety of scatterers present.

2.2.2 Multiple Particle Scattering Models

When the number of distinct interactions is very large, as in turbid media such as a cloud, milk, or tissue models above are not feasible because light propagation do not behave like a propagating wave or a ray, but like erratically moving photons migrating on average through the medium. So a technique that models the large number of interactions by some aggregate approach is required such as radiative transport theory (RTE). In this approach light is treated as composed of distinct particles, photons, propagating through a medium modelled as a background which has constant or variable scattering and absorption characteristics, possibly containing discrete, bounded regions of absorption and/or scattering inhomogeneity. Interactions between light particles and the medium only are modelled and not among light particles themselves. Thus there is no correlation between the fields the particles represent; consequently powers, instead of fields, are additive [6].

$$\begin{aligned} &\frac{1}{v}\frac{\partial L(\mathbf{r},\hat{\mathbf{s}},t)}{\partial t} + \hat{\boldsymbol{s}}\cdot\nabla L(\mathbf{r},\hat{\mathbf{s}},t) + \mu_t L(\mathbf{r},\hat{\mathbf{s}},t) \\ &= \mu_s \int_{4\pi} p(\hat{\mathbf{s}},\hat{\mathbf{s}}') L(\mathbf{r},\hat{\mathbf{s}}',t)\, d\hat{\mathbf{s}}' + Q(\mathbf{r},\hat{\mathbf{s}},t) \end{aligned} \tag{2.9}$$

Where, $L(\mathbf{r},\hat{\boldsymbol{s}},t)$ is the radiance (the power per unit area and unit solid angle) at position $\mathbf{r}$ in the direction $\hat{\boldsymbol{s}}$, at time t. $\mu_t = \mu_s + \mu_a$, are the optical transport, scattering and absorption coefficients respectively, $p(\hat{\mathbf{s}},\hat{\mathbf{s}}')$ is the scattering phase function and $Q(\mathbf{r},\hat{\mathbf{s}},t)$ is the radiant source function. *v is* the electromagnetic propagation speed in the medium.

Transport theory deals directly with the transport of energy through a medium containing particles. The formulation is flexible and capable of treating many physical phenomena. It has been successfully employed for the problems of atmospheric and underwater visibility etc. [7]. If we consider a small element in space at r, the first term on the left-hand side is the time derivative of the radiance, the second term accounts for the flux of photons along the direction $\hat{\boldsymbol{s}}$, third term accounts for scattering and absorption losses from the element; left-hand side of Eq. 2.9 accounts for photons leaving the element. On the right hand-side, the first term; integral accounts for photons at position r being scattered from all directions $\hat{\boldsymbol{s}}'$ into direction $\hat{\boldsymbol{s}}$, the second term is the photon source; right- hand side of Eq. 2.9 accounts for photons entering the small element [6, 8].

Linear transport equation is applicable to a wide range of media, but analytical solutions are only available for simple scenarios because of the integro-differential structure of the equation. Numerical solutions to the linear transport equation are computationally intensive due to the dependence on space, angle, and time [6].

Simplification of linear transport equation is possible when the reduced scattering coefficient of the medium is much bigger than the absorption coefficient and when the radiance is almost angularly uniform, having only a relatively small flux in any particular angular direction. Diffusion approximation to linear transport theory results in the variable-scattering form of what is known as the photon diffusion equation:

$$\frac{1}{v}\frac{\partial \Phi(\mathbf{r},t)}{\partial t} + D\nabla^2\Phi(\mathbf{r},t) + \mu_a\Phi(\mathbf{r},t) = S(\mathbf{r},t) \tag{2.10}$$

where, $\Phi(r, t)$ is photon fluence rate, $S(r, t)$ is the equivalent isotropic source and $D=v/[3(\mu_a+\mu_s')]$ is the diffusion coefficient [6, 8]. Diffusion approximation is valid if:

- There are no interactions between photons
- Scatterers and absorbers are discrete and do not interact
- Radiance at any point is isotropic, there is only a small forward flux
- $\mu_a << \mu_s'$
- Source - detector separation $>>1/\mu_s'$
- Distribution of light is static with time (for our case)
- All media have homogenous optical properties
- Tissue has a uniform index of refraction (light will travel in a straight path) [6, 9].

Diffusion theory is well suited for modeling optical transport through tissue, where scattering predominates and the nature and geometry of the scatterers on a subcellular scale is never known. An example of an empirical extinction measurement is shown in Figure 2.2, which matches diffusion theory predictions. Collimated light beam rapidly loose direction and turn into an isotropically diffusing beam within a depth of about 5 mm.

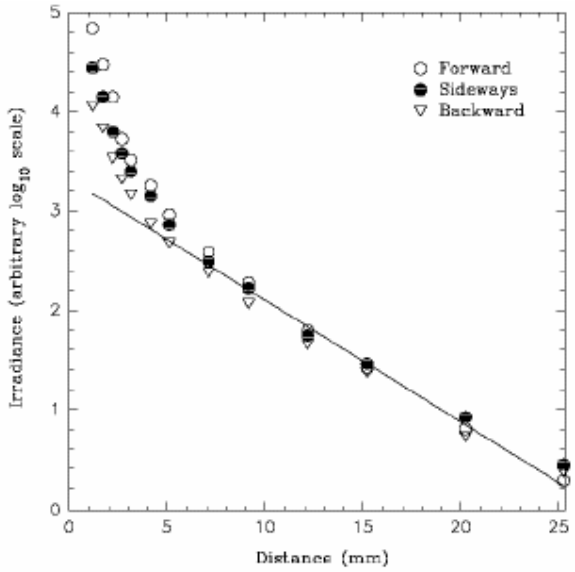

Figure 2.2 Irradiance vs. depth in post-mortem neonatal brain tissue at λ = 660nm [4].

2.3 Major Optical Absorbers and Scatterers in Tissue

Any compound which absorbs light in a spectral region of interest is known as a *chromophore*. Each chromophore has its own particular absorption spectrum which describes the level of absorption at each wavelength. The principle chromophores in tissue are water, lipids, melanin, haemoglobin, bilirubin and cytochrome oxidase. Concentration of water, lipids, melanin and bilirubin remain virtually constant with time however oxygenated haemoglobin (HbO_2), deoxyhaemoglobin (Hb), and oxidised cytochrome oxidase (CtOx), have concentrations in tissue which are strongly linked to tissue oxygenation and metabolism. There are also other forms of hemoglobin (HbCO, Hi, SHb) which have a lower absorption spectra and ignored, ineffective at transporting oxygen, and are usually formed as a result of a metabolic disorder.

Water which constitutes %60-80 of human body obstructs spectroscopic interrogation above 900 nm because of its dominant absorption (Figure 2.3). Below 650 nm there is an overwhelming absorption of Hb. In a spectral window, at 650 – 900 nm, light which has traversed up to 8cm of tissue can be detected with sensitive instrumentation. This is near – infrared (NIR) region of electromagnetic spectrum.

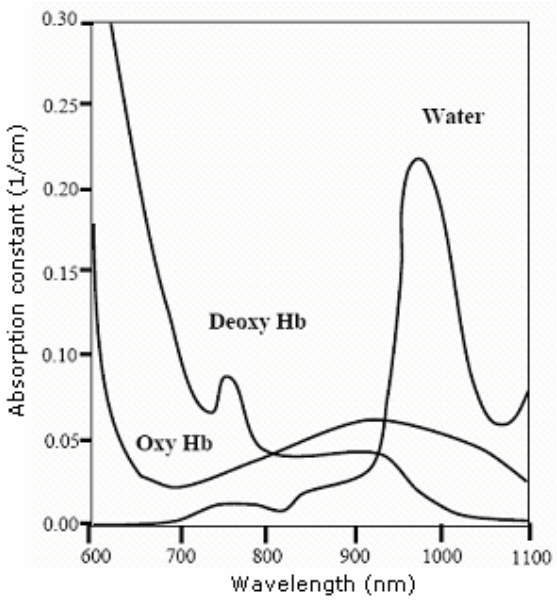

Figure 2.3 Absorption spectra of water, haemoglobin and oxy – haemoglobin showing their absorption of light with wavelengths 600 to 1100 nm [10].

Moreover, within this window the spectra of oxy- and deoxy –hemoglobin are distinct enough to offer the possibility of performing spectroscopy (Figure 2.4). This fortunate situation is the basis of functional NIRS (fNIRS) and DOT technologies. Figure 2.4 shows the isosbestic point at ~805nm. Optical measurements at this wavelength are sensitive to total blood volume and are unaffected by changes in oxygen saturation.

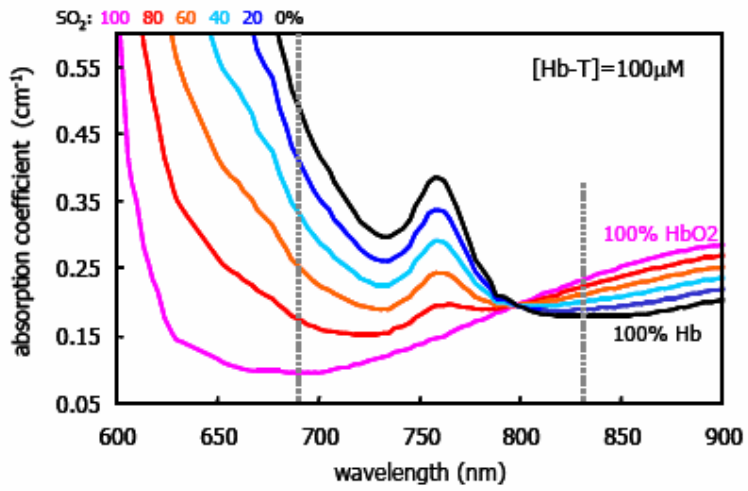

Figure 2.4 Spectral absorption properties of blood as a function of oxygen saturation [4].

Biological media is highly scattering, and consists of both optically static (connective tissue, collagen, skin, etc.) and optically dynamic (neurons, while firing) scatterers. The static scatterers dominate, and are responsible for the creation of the diffuse optical probability density function within the tissue. Dynamic scattering changes in neurons during activation are thought to be capable of generating minute changes in the optical pathlength that can be detected noninvasively with RF and CW DOT instrumentation. Mitochondria compose up to 20% of the total solid content within the cells are a significant scattering source.

2.4 Modeling the Medium – Forward Problem

Algorithm for forward problem provides a weight (or importance) to each voxel within the sample volume, and the measured signal is a function of these weights. One can think of the weights as being proportional to the probability of photons from a source reaching a particular voxel, and then continuing on to reach the detector position.

Direct approaches for modeling the medium are analytical solutions and Monte Carlo simulations. Analytical solutions can generate weights for a homogeneous system with an embedded spherical or cylindrical object. Monte Carlo simulation is the most precise but time-consuming method of generating the weights. The advantage of these calculations is that they can accurately model irregular boundary conditions and heterogeneous media.

Numerical methods involve for approximation of partial differential equations by such as finite element and finite difference approximations. They are based upon linear perturbation approaches such as the Born and Rytov expansions. They relate the absorption coefficient to the measured data through a linear system of equations.

2.5 Distribution of photon paths

Knowledge of the distribution of photon paths is important in absolute quantitation of many measurements in light transport through tissue systems and in identifying which cells dominate the detected photon signals.

Experimental data show that the incident photons from the source fiber migrate to the detector fiber in semi-infinite geometry through paths whose distribution in space resembles the shape of a "banana", with its two ends connecting the source and the detector and its middle portion extending to the deepest part of the sample. The re-emitted photon paths have maximum probability in the core of banana (Figure 2.5) [11].

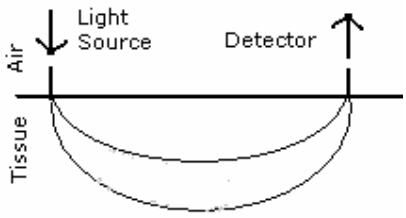

Figure 2.5 So called 'banana' path distribution of diffuse photons. This is primarily due to the reflective geometry and small and plane detector area.

2.5.1 Maximum Depth of Banana Pattern

For a homogeneous medium photon diffusion equation in Eq. 2.10 for a DC point source gives the familiar solution

$$\Phi_0(r) = \frac{S_0}{4\pi D}\frac{\exp(-\kappa|\vec{r}-\vec{r}_0|)}{|\vec{r}-\vec{r}_0|} \tag{2.11}$$

where, $\kappa \equiv 1/L_a = \sqrt{\mu_a/D} = \sqrt{3\mu_a\mu_s'}$ is the inverse diffusive absorption distance. In the multiple scattering regimes, it is the distance scale L_a that determines the range of diffusive light migration in space, as opposed to $1/\mu_a$, which determines the decay of light through transparent medium [11].

For the homogenous semi-infinite geometry, solution is

$$\Phi_o(r) = \frac{S_0}{4\pi D}\left(\frac{\exp(-\kappa|\vec{r}-z_0\hat{z}|)}{|\vec{r}-z_0\hat{z}|} - \frac{\exp(-\kappa|\vec{r}+z_0\hat{z}|)}{|\vec{r}+z_0\hat{z}|}\right) \tag{2.12}$$

Our boundary condition is at z = 0; Φ = 0, putting the source for diffusive photons at $\vec{r}_0 = (0, 0, z_0)$, where z_0 is the distance depending on the precise nature of the sample.

It is possible to derive the formula P(x, y, z) for the photon density distribution at $\vec{r}_1$=(x, y, z) (for the photons injected at $\vec{r}_0$ = (0, 0, 0) and detected at $\vec{r}$ =(r, 0, 0))[11]. At the center line of the "banana" region, this function will give maximum values, let us denote this center line z_0 (x)[11]. This line will reach its maximum depth z_0^{max} at x = r/2 (at the middle of the source and detector distance), which is, in the weak absorption limit κr << 1;

$$z_0^{max} \approx \frac{\sqrt{2}}{4} r \tag{2.13}$$

where r is the source –detector separation. In the strong absorption limit for κr >>1,

$$z_0^{max} \approx \sqrt{\frac{r}{2\kappa}} \quad [11]. \tag{2.14}$$

Banana regions become much narrower as absorption is increased. For a low absorbing medium it can be said that banana region is independent of optical properties of the medium (Eq. 2.13).

2.5.2 Effect of Source Detector Separations

The photon diffusion equation provides useful insight into the relative sensitivities of the surface fluence to changes in μ_a and μ_s when measurements are made at different source-detector separations.

In the diffusion limit the flux exiting the semi-infinite medium normal to the surface is given by;

$$R(\rho) = \frac{z_0 A_d}{2\pi}\left[\frac{\alpha}{\rho^2 + z_0^2} + \frac{1}{(\rho^2 + z_0^2)^{3/2}}\right]\exp\left[-\alpha(\rho^2 + z_0^2)^{1/2}\right] \tag{2.15}$$

where $z_0 = K / \mu_s'$ is the extrapolation length, A_d is the area of the detector, ρ is the separation between source and detector probes and $\alpha = \sqrt{3\mu_a(\mu_s' + \mu_a)} \approx \sqrt{3\mu_a\mu_s'}$ for $\mu_a << \mu_s'$ (Figure 2.6)[12]. *K* is a dimensionless constant with a magnitude that depends on the anisotropy parameter of the scatterers and the reflection coefficient at the surface. At large source–detector separations, Eq. 2.15 simplifies to:

$$R(\rho) = \frac{\sqrt{3}A_d}{2\pi\rho^2}\sqrt{\frac{\mu_a}{\mu_s'}}\exp(-\alpha\rho) \tag{2.16}$$

for $\rho \gg 1/\alpha \gg z_0$ and $\mu_a \ll \mu_s'$ [12].

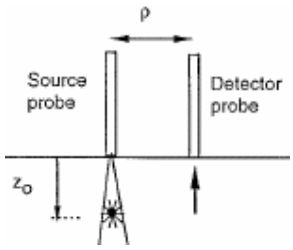

Figure 2.6 In reflective mode, incident light from the collimated source is converted to a diffuse source located at a depth z_0 one extrapolation length below the surface and the photon fluence normal to the surface is captured by the detector, where ρ is the source and detector probes distance [12].

2.5.3 Electrostatic Analogy

Photon is the name given to a quantum of light or other electromagnetic radiation. The photon is the exchange particle responsible for the electromagnetic force. Many everyday forces, such as friction, and magnetism, are caused by the electromagnetic force. Since photon is the carrier particle for both radiation and electrostatics it is convenient to make the analogy of dipole electric field for light diffusion in a semi – infinite medium (Figure 2.7).

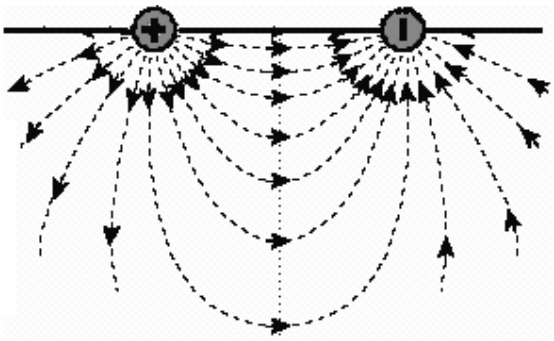

Figure 2.7 Imaginary electric field lines of an electric dipole in a supposed semi – infinite medium. Along a line magnitude of electric field is constant.

Electric filed due to a point charge q, at a distance r is;

$$E = \frac{1}{4\pi\varepsilon_0}\frac{q}{r^2} \tag{2.17}$$

where, ε_0 is the *permittivity constant* for *space* which is a physical quantity that describes how an electric field affects and is affected by a medium.

Electric field due to a dipole is,

$$E = \frac{1}{4\pi\varepsilon_0}\frac{p}{(a^2 + r^2)^{3/2}}, \tag{2.18}$$

p = q(2a) which is an intrinsic quality of a dipole, is directly related to the magnitude of the charges and their distance to each other, r is the distance of the point from the midline of the dipole (Figure 2.8).

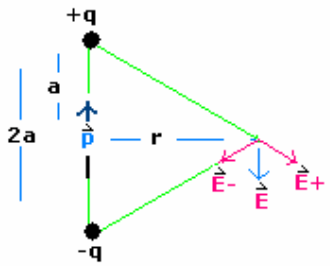

Figure 2.8 Electric field that is formed when positive and a negative charge with equal magnitude are placed at a distance 2a.

Electromagnetic force has infinite range which is owed to the zero rest mass of the photon. Eq. 2.18 is quite similar to Eq. 2.11, for instance optical properties of medium are described by D, and electrical properties of the medium are by ε.

2.6 Medical Imaging Modalities

2.6.1 Ballistic Imaging

Most neuroimaging tools in use today operate in a ballistic fashion. The term "ballistic" imaging refers to all modalities in which the excitation energy travels in a straight line from the source through the sample and from the sample to the detector. As a result, all ballistic imaging modalities generate well-posed analytical problems (i.e. problems in which the number of measurements is always sufficient to reconstruct an image). Examples of other ballistic imaging modalities include endoscopy, microscopy, optical coherence tomography, X-ray, CT, video fluoroscopy, PET, ultrasound, and fMRI.

Ballistic methods can form high-resolution images. Image quality can be uniform throughout the entire sample volume, while with DOT the spatial resolution decreases with increasing depth, as the PDF diverges (Figure 2.9).

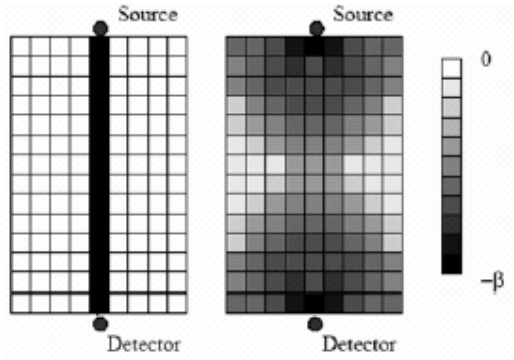

Figure 2.9 Weight distributions for C-T (left) and DOT in transmission-mode (right) [4]

The DOT distribution is a broad probability density function, while the C-T distribution gives equal non-zero weights along the source-detector line of sight and zero weights elsewhere (Figure 2.9).

Most ballistic modalities provide excellent structural detail but only limited metabolic information. They are either far too slow for imaging hemodynamic events in real-time, or do not measure oxygen (fMRI). Photon energies must be very high, which can deposit tens of eV per collision that can break covalent bonds within most of the biomolecules easily. Random scission of biomolecules can lead to autosomal mutations, cell death, and cancer.

2.6.2 Diffuse Optical Imaging

Since transmitted or reflected light re-emerging from the tissue has followed a very complicated path, any localization of absorption or scattering or other optical parameters is lost when we simply observe the light as it exits the tissue. DOT forms maps of absorbers and scatterers predicting the way photons travel within tissue. Steps of DOT are summarized in Figure 2.10.

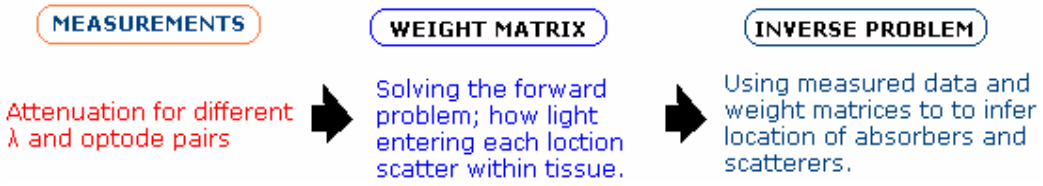

Figure 2.10 How to acquire images with diffuse photons.

The optical properties are then used to determine blood volume and oxygenation changes, which are typically plotted as 2-D spatial images for a given depth. Since DOT measurements can be acquired rapidly, these data can be acquired at frame rates fast enough to capture the temporal evolution of the hemodynamic response.

There are several measurement techniques and modes. The simplest of three common techniques involves performing an amplitude-only measurement, and is referred to as continuous wave, or "CW" Second one, the "RF" technique measures both amplitude and transit time in the *frequency domain* using RF-modulated light sources. The "time-domain" technique uses sub-nanosecond optical pulses to measure both amplitude and transit time within the *time domain*.

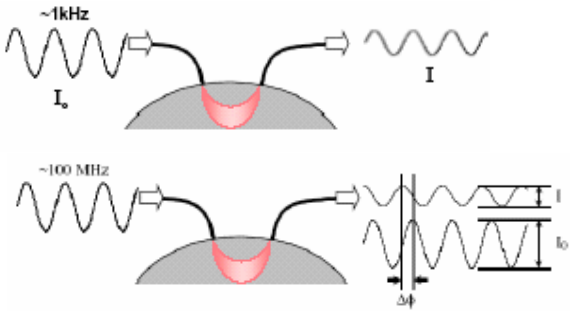

Figure 2.11 Representation of a CW (top) and an RF (bottom) instrument, with an RF instrument time delay due to diffusion can be determined. This delay creates a measurable phase shift in the modulation envelope of the detected light relative to the light entering the tissue [4].

CW instrumentation: Continuous-wave instruments are the easiest to build and operate. CW systems emit at constant amplitude, or are modulated at frequencies not higher than a few tens of kilohertz, and measure only the amplitude decay of the incident light Figure 2.11 (top). Lock – in technique is used to detect and measure very small AC signals. A Lock – in amplifier can make accurate measurements of small signals even when the signals are obscured by noise sources which may be a thousand times larger [13].

RF instrumentation: RF-modulated DOT instruments are much more complex to build than CW instruments, but they offer the capability to measure both amplitude changes and transit time changes in the light traveling between each optode pair Figure 2.11 (bottom). In RF systems the light source is on continuously, but is amplitude-modulated at frequencies on the order of tens to hundreds of megahertz [4].

Time-domain instrumentation: With a time-domain instrument, sub-nanosecond laser pulses enter the tissue and are simultaneously attenuated and broadened as a result of absorption and temporal dispersion due to scattering within the tissue. The shape of this distribution provides information about tissue optical parameters. Optical attenuation can be measured as a direct function of photon transit [4].

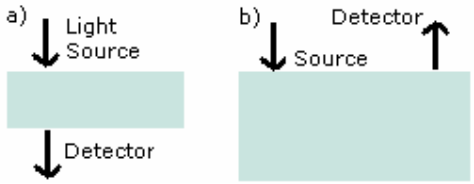

Figure 2.12 Two modes of DOT, a) transmissive, b) reflective. In a reflective mode only photons that are reflected are used.

Three most common modes are transmissive, reflective and annular in which sources and detectors form rings (Figure 2.12) [6].

2.7 Applications of DOT

The most important current applications of DOT are detecting tumours in the breast and imaging the brain. The greater blood supply of tumours compared to surrounding tissue provides a target absorption inhomogeneity to image. A similar idea allows us to image bleeding in the brain or do functional imaging with the same association between cerebral activity and increased oxygen supply as used in functional magnetic resonance imaging (fMRI). In addition relative Hb/HbO concentration may not only differentiate tumours from background tissue but also may discriminate among tumours with different activity rates. DOT can potentially enable the necessary early diagnosis/discrimination between ischemic and hemorrhagic stroke, which is critical for drug treatment, and patients' life. Furthermore, DOT may allow continuous bedside monitoring of the evolution of stroke as well as its response to treatment.

3. METHOD

Computer simulations and experiments detecting light entering and propagating inside the medium in a reflective geometry is evaluated in the aim of searching,

- Change of detected fluence with screen perturbations on the path of photons
- Effect of increasing light power on banana pattern
- Effect of increasing light power on probing depth
- If light power and fluence relation can be used as an imaging tool

In both, coherent 850 nm light source is used without modulation.

3.1 PMI Simulations

Computer simulations are done at Matlab, with the Photon Migration Imaging (PMI) Toolbox[1] which implements numerous algorithms for performing the forward and inverse calculations associated with diffusive optical imaging [14]. Here we are not concerned with inverse calculations. PMI solves the forward problem of light propagation in the media with diffusion approximation to RTE, models the medium with finite elements method with selected perturbation approach. PMI first calculates initial fluence for homogenous medium than calculates total perturbed fluence for a given perturbation. Each cell defines a single perturbation [15]. When the optical properties are spatially varying there are two standard linear approaches for finding approximate solutions: Born and Rytov approximations [16].

The first Born approximation expresses the total fluence rate or total field as a combination of the incident field (the field that would have been detected if no optical heterogeneity was present) and the scattered field (the field attributed only to the heterogeneous optical distribution).

$$\Phi = \Phi o + \Phi pert \qquad (3.1)$$

The Born approximation makes the assumption that the scattered wave is small, and that it scales approximately linearly with the absorption. In biological tissue we are

[1]Available at: http://www.nmr.mgh.harvard.edu/PMI/toolbox/index.html

interested in imaging absorption values that vary from about 0.02 cm^{-1} to 0.30 cm^{-1}. In fact, this linear assumption will break down for absorption differences greater than about 0.10 cm^{-1}, which is well within our region of interest. *The Rytov approximation*

$$\Phi = \Phi o \exp(\Phi pert) \qquad (3.2)$$

does not place a restriction on the magnitude of the scattered wave change, but rather assumes that the scattered field is slowly varying [4, 17]. Thus, for many tissue-imaging situations, it is better to use the Rytov approximation.

Rytov approximation is chosen because of its advantages. This approach neglects secondary scattering effects, takes into account only first scatter. With PMI it is also possible to use non-linear approaches for multiscattering photon propagation.

Table 3.1
Features of PMI simulations.

Slab geometry (cm^3)	10x10x7.5
Optical properties of medium (1/cm)	$\mu_a = 0.044$ $\mu_s' = 9.3$ Index of Refraction = 1.33
Optical properties of perturbation layer (1/cm)	$3\mu_a$
Wavelength of light (nm)	850
Modulation Frequency	0
Perturbation Approximations	Rytov
Computational volume of voxels (mm^3)	5x5x5

General features of Simulations are summarized in Table 3.1. We take the source function to be constant in time, i.e. we are concentrating to DC case.

3.1.1 Problems Encountered During Simulations

In the first simulations, to form screens that absorb photons totally (Figure 3.1 left), their μa values are chosen close to or higher than μs' values, which violates primary condition of diffusion approximation: $\mu a << \mu s'$. We assumed the effect would be small by choosing the width of screen infinitesimal. This gives acceptable results. After having experimental results and comparing the two, it is understood that actually, to describe this

phenomena screen application is not the correct way. PMI inevitably blows up, since we have violated the assumption.

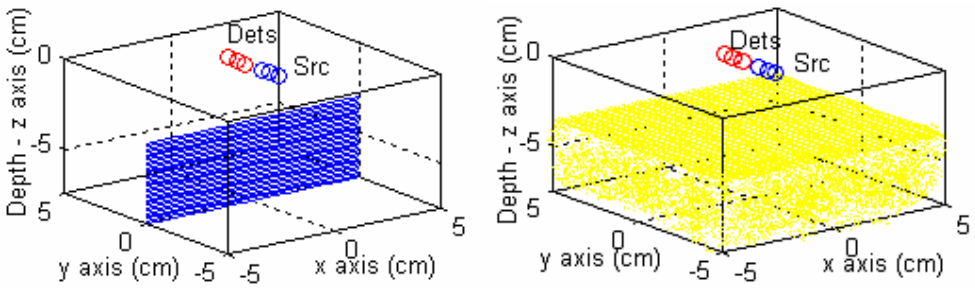

Figure 3.1 Simulation geometry with screen (left) and layer (right) perturbations.

Since our approximation takes into account only first scatter, it is possible to design layers with different depths instead of putting screens as perturbation. This approach gave better results and similar to experimental ones. However it is learned that diffusion approximation gave 10% error in paths of photons for slab geometries less deep than 1 cm [18]. Also we assumed the borders (walls) of the geometry as absorbers but could not find evidence. So it is decided to use a layer to form a perturbation, which is assumed to give results resembling a screen perturbation. The μ_a of layer is chosen three times higher than the mediums, which is enough to intersect light below the interface and does not violate diffusion approximations rule (Figure 3.1 right).

PMI Toolbox provides necessary documentation and sample codes. Although it is rigorously prepared there is an error in 'PMI2\Doc\example1.m'. The code generates data and constructs images. However when you run the code you will encounter the error message:

```
Error in ==> C:PMI2\Doc\example1.m
On line 176 ==>    X = reshape(X, nVox, 2*nWvl);
```

You will have to change the factor '2' of 'nWvl' with '4', then the code runs.

3.2 Experiments

During experiments metal sheets at different heights are put as absolute absorbers in the phantom. It is known that the depth of banana pattern for different SD pairs is different (Figure 3.2). Nevertheless, the dependence of depth for an SD pair to incident

light power is unknown. Adjusting the output power of the laser, for different inputs and for different source – detector separations, output fluence of diffuse light that is captured with the detector fiber is measured at the oscilloscope.

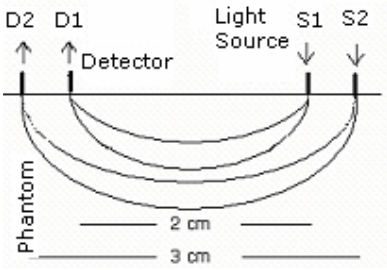

Figure 3.2 Diffuse photon paths of 2 cm and 3 cm pairs have different depths.

3.2.1 Preparation of Experimental Set – up

Organization and elements of Photon Migration Experiment set – up is summarized in Figure 3.3 – 3.4 below.

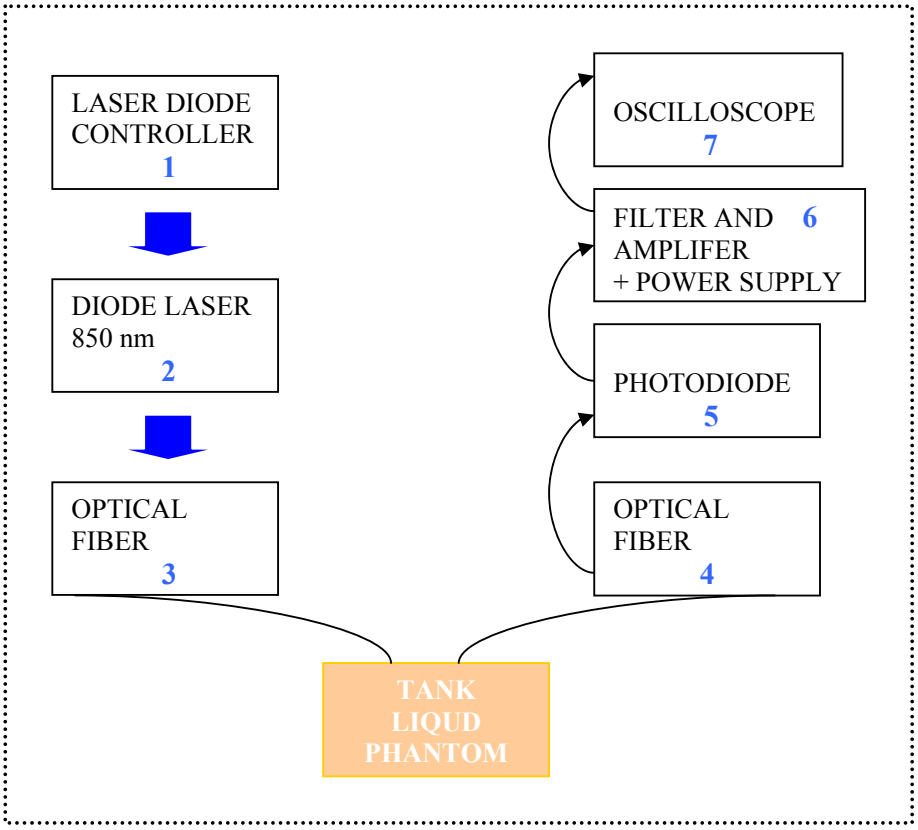

Figure 3.3 Elements of photon migration experiment set – up in order.

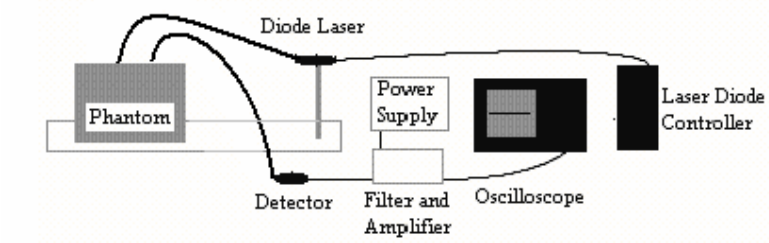

Figure 3.4 General look of our set – up.

1. Laser Diode Controller

LDC 500 laser diode controller by Thorlabs is used for the operation of the laser diode. LDC works between 0-500mA. It regulates the laser current, means; laser output power [19].

2. Diode laser – (focusing tube, laser mount, post and post holder)

L850P030 Thorlabs, 850 nm diode laser is used. Due to diffraction, the beam diverges (expands) rapidly after leaving the chip, typically at 30 degrees vertically by 10 degrees laterally. A collimating lens (focusing tube) must be used in order to form a collimated beam. Laser with a focusing tube is mounted in a translating mount with a post and post holder to fix it on a plane.

3-4. Optical fiber

Industrial Fibers, jacketed, plastic 1 mm (core) diameter, multimode communication fibers are used. Two factors are important for efficient light delivery in an optic system. If it is the case of a laser diode, the connection (coupling) of laser and the fiber and the fiber ends. SMA connector, a screw on type connector, is used for coupling of both laser – fiber and fiber – photodiode couples. Fiber ends should be smooth and nicely cut. By a small handy tool that leaves the edge of the fiber out, fiber can be polished on a sand paper. This is a cheap and efficient way of smoothing fiber ends. To control you can put the end of the fiber to light and will see the bright light output coming out of the other end.

5. Photodiode

SM05PD1A, Thorlabs silicon photodiode is used. SM05PD1A has a reasonable active area, a high responsivity for 850 nm light, which is determined by the material it is

made from (silicon). It is just a photodiode not a photodetector; is not biased. So it operates in the photovoltaic mode, gives electricity as output. The electric signal has to be applied across a high resistance in order to be seen as a voltage difference, like in our case an oscilloscope. A photodiode can be operated in photovoltaic or in biased mode. Photodiodes operated in the photovoltaic mode normally have extremely low noise, but the price to be paid for low noise is very slow response times. On the other hand, photodiodes operated in a biased mode will have faster response times, but the noise will be larger [20].

6. Filter and amplifier circuit

To see a noise free and higher signal on the oscilloscope, a circuit to filter especially the mains 50 Hz noise (notch filter) with an amplifier, which amplifies the signal ten times, is designed. This circuit employs two operational amplifiers and to feed the circuit a power supply at ±7 volt. The signal of the circuit for day light coming from the detector fiber can be seen directly on the oscilloscope in 1-2V range which is very high for an optical set – up.

7. Tektronix TDS 1002 oscilloscope; measurements are done for DC voltage at 2V and 10 ms range.

3.2.2 The Liquid Phantom

Intralipid (10%) (Fresenius Kabi, 500 ml , 2005) is used as a turbid medium[2]. Intralipid is a phospholipid emulsion used for intravenous feeding of hospitalized patients. There are 10% and 20% emulsions available where percentage is defining the fat content. It is a polydisperse suspension of particles with an average diameter of 0.4 μm but a relatively wide range of sizes i.e. from 0.1μm m to 1.1 μm (Table D.1) (Figure B.2)[21].

Particle characteristics governing its scattering properties are radius and refractive index. The anisotropy parameter is also strongly dependent on the size distribution, tending to higher values as the particle size increases. Also the scattering characteristics of large particles show almost no dependence on wavelength, while of particles with diameters comparable to the wavelength or smaller show a strong dependence on wavelength, μs' decreases with λ.

[2] Efeoğlu Eczanesi, Millet Cad. No: 131/Çapa/Istanbul.

Intralipid is turbid and has no strong absorption bands in the visible region of the electromagnetic spectrum; it is possible to measure diffuse light. There are several brands of intralipid available worldwide and its optical properties are well-studied i.e. total attenuation coefficient varies from 575 to 150 cm-1 between 500 and 890 nm [22].

Intralipid (10%) is too dense to be used directly. Pure water, which is distilled using *reverse osmosis separation technology* in the Department of Molecular Biology and Genetics, is used to prepare a 10% diluted solution of intralipid (10%). Distilled water is an absorber but does not have any scattering content.

According to van Staveren et al. reduced scattering coefficient of intalipid (10%) at 850 nm is, $\mu_s' = 93\ cm^{-1}$ [23, 24]. We had the chance to determine the optical properties of the intralipid in the Biophotonics Laboratory; results did not match the literature so we decided to use literature values. Determination of optical properties by van Staveren et al. was based on electron microscopy to study the size and distribution of the particles. They used Mie theory to calculate the optical properties. These calculations were compared to the optical properties measured experimentally. Total attenuation of collimated light was measured. They derived simple expressions for μ_s and g of intralipid at different wavelengths which approximate the Mie theory solutions.

Diluted intalipid is expected to have a lower scattering coefficient than the original; g does not depend on concentration but particle properties. Eq. 2.1 tell us that μs' is directly proportional to number of scatterers. Since pure water has no scattering contribution, the number of the scatterers per volume decreases directly proportional to the volume of the all solution. μ_s' of the diluted solution at 850 nm will be

$$\mu_{s\,(solution)}' = \frac{\mu_{s\,(water)}' V_{(intralipid)}}{V_{(solution)}} = 93/10 = 9.3\ 1/cm \qquad (3.3)$$

μ_a of the solution is approximately same as the water's. From Eq. 2.5 absorption coefficient of the diluted intalipid solution at 850 nm is,

$$\mu_{a(solution)} = \frac{\mu_{a(intralipid)} V_{(intralipid)} + \mu_{a(water)} V_{(water)}}{V_{(solution)}} \simeq 0.044\ 1/cm \qquad (3.4)$$

Here absorption coefficient of water is taken on basis of natural logarithm, but there are sources that take on log 10 bases [25]. Care must be given to the base that is used because log10 base attenuation differs from ln base attenuation by a factor of ln (10) ≈ 2.3. Optical properties of human tissue and intralipid with natural logarithm base are summarized in Table 3.2.

Table 3.2
Optical properties of human tissue and intralipid (10%) 10% diluted solution for 850 nm. [25, 26]

	μ_a cm^{-1}	μ_s 'cm^{-1}	Ref. Index
Dermis	0,122336	17,57397	≈1.4
Fat	0,085898	11,0916	
Muscle	0,295342	6,59788	
Water	0.044	-	1.33
Intralipid (10%) Solution 10%	0.044	9.3	≈1.33

Intralipid is milk-like nutrient and has to be kept in the fridge (Figure B.2).

3.2.3 Tank

Phantom tank is made from dark plexiglass (10x10x7.5 cm^3). Small holes, 2.2 mm in diameter, are drilled on the cover for the source and detector fibers. Its structure enables us to put a metal screen and fix its position inside (Fig. 3.5 and Fig. B.1). Light detected by the detector inside the tank for the dark environment is zero.

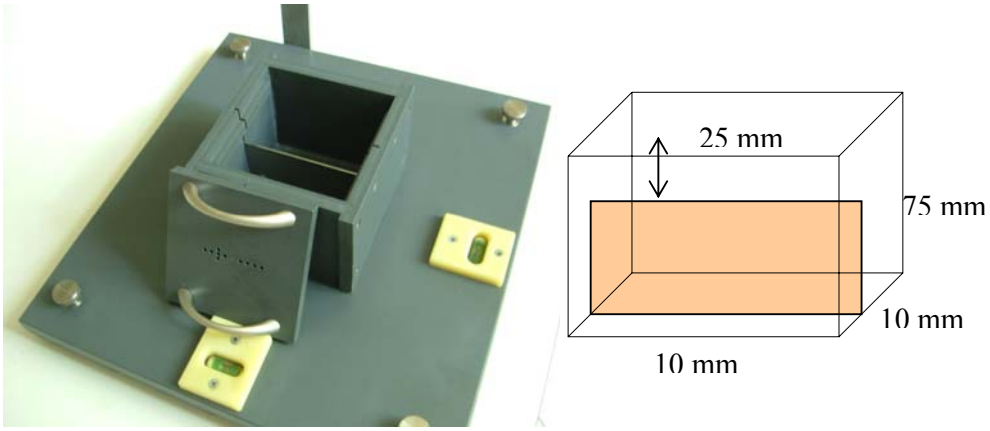

Figure 3.5 Phantom tank and tank cover with a metal screen 25 mm below the surface (left) and representation of the tank (right).

3.2.4 Calibration

Calibration process involved optimization of fiber – laser, fiber – photodiode couplings, fiber ends, and determining system characteristics. After optimization I observed up to 25% increase in output.

- Systems stability is tested for three hours and seen that by time laser output did not change significantly.
- Laser output becomes stable 5 - 10 minutes after turning on.
- Set up is sensitive to position changes; nothing should be touched during experimentation.
- There are three detector fibers from phantom to photodiode to get a larger total detection area. They are controlled for their giving same output for an input. There is a 0.5% difference, which is not significant.
- Screens are metals and their surface can scatter visible light. It is checked for 850 nm; covering the screens with black plastic did not change the measurements.
- Filters ability to filter 50Hz signal is controlled.
- Our laboratory is hosting many other devices including UPS, which serves the department for electric shortages. There is substantial noise due to the environment. To alter this problem we used a Faraday cage.
- Diluting intralipid yielded at least 50 % increase in the output.
- If there is a gap between fibers and intralipid solutions surface this causes an increase in light output due to reflection from the surface. It is important to make sure that fiber ends touch the phantom and are at the same level. For this, fibers are marked with wires above tanks cover.
- Change of temperature of the phantom can effect measurements. With the non contact infrared thermometer intralipids surface temperature is measured before and after a long-time of experimentation. Exposure to laser long time did not raise intralipids temperature; this is because of its low absorption at 850 nm.
- The tank is adjusted to be just parallel to earth, which is important for the leveling of liquid inside.
- Output of the laser is measured with a powermeter (Thorlabs S120). The laser output from the fiber that the phantom sees at 65 mA is 0.42 mW on average. The

laser output is 7 mW at 60 mA. A 1/20 decrease is very acceptable if we consider that diameter of the input fiber is 1mm (core) and a small percentage of light is attenuated in the fiber also.

- From Figure F.2 it can be seen that laser works linearly at 65-75 mA. Measurements are taken at that interval.
- Photo diode – filter –amplifier systems unlinearity is displayed in Figure F.3
- There are more than one system in this set up, to name; photodiode, fibers, circuit and oscilloscope. All this systems change the signal until it is seen on the oscilloscope. We needed to calibrate the data that we measured from the system, so that input and output would have the same units like there is only one system that measures. To do so a curve that interprets the 'Current' we see on the laser diode driver to 'Voltage' on the oscilloscope is acquired and all input light data is interpreted in 'mV' according to this data, not in 'mA's (Table 3.3).

Table 3.3

Output of laser diode currents from the input fiber end

Laser Diode Current (mA)	Output by Oscilloscope (V)	Output by Powermeter (mW)
65	4.176	0.23
70	4.386	0.35
75	4.53	0.44
80	4.638	0.54

3.2.3 Problems encountered during experimentation

Laser – output graph was linear up to 80 mA but beyond it was very chaotic. We expected the laser to work at 100 mA max according to data sheet. Thinking laser was damaged it is understood that there are two data sheets available, one of which belongs to our laser – the older one which should work at 80 mA max., newly produced L850P030 lasers are working at 100 mA max.

There were times that the signal is not stable with an unknown reason then measurements are not taken.

Experimental procedure involves opening the tank cover and changing screens, and changing fiber positions. This was affecting the consistency of the experiments. A position

adjuster is designed with 55 mm screen. With this millimeters sensitive tool it is possible to move the screen upwards and downwards to a desired height. Later the same tool with a 20 mm screen is used to determine the sensitivity of photon path for this set – up.

4. RESULTS

Simulation parameters were adjusted to match experimental findings. Throughout this chapter simulation results will be presented first then experimental results will proceed.

4.1 PMI Simulations

4.1.1 Homogenous Medium

It is well known that number of photons in a diffusive medium does not change the way interactions happen, meaning; optical interactions happen one by one and do not affect each other. Moreover to make the diffusion approximation possible interactions of photons with each other are ignored. As a result we expected a linear relation between light output and input power by the simulation, which is shown in Figure 4.1.

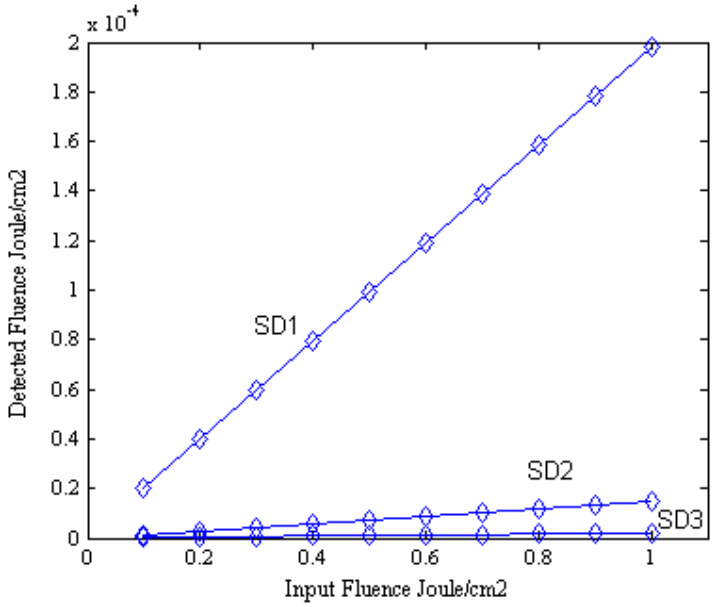

Figure 4.1 Source – detector (SD) pair with 1 cm distance (SD1), with 2 cm distance (SD2) and with 3 cm distance (SD3) outputs for increasing input power.

It is clearly seen that source – detector (SD) pairs with increasing distance have slopes in descending order (Figure 4.1). This was expected due to increasing path of photons and as a result of being subject to more absorption. Secondly, output of a distant detector is lower than a nearby one. How does mean photon path change with SD

separation? Since we are dealing with a homogenous medium we can employ Beer – Lambert law to find out the mean photon path. Eq. 2.6 gives us this simplistic input output relationship:

$$A = \ln [Io / I] = \mu_a.d.\ DPF + G \qquad (4.1)$$

Here, 'd' is the optical path, 'd. DPF' is modified path due to scattering and G is dependent upon the measurement geometry which is unknown. For a highly scattering homogenous medium where optical properties and G are constant, A is related to optical path. Figure 4.2 have two important findings; i) optical mean pathlength is not a function of incident light intensity, ii) but it is proportional to SD separation.

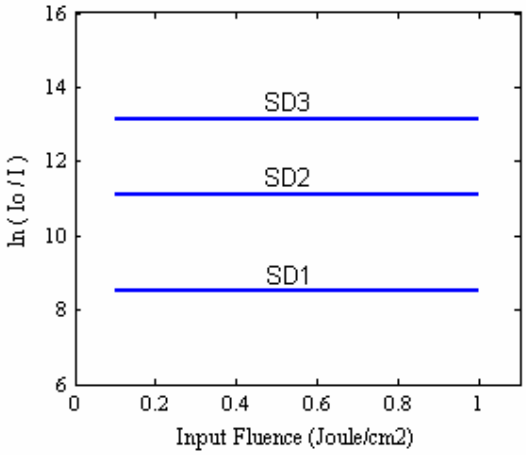

Figure 4.2 Optical mean pathlength increases as SD distance increases.

Attenuation decreases as SD separation decrease but this decrement is not linear, SD3 – SD2 difference is bigger than SD2 – SD1 difference, this is the clue for an exponential relation. Eq. 2.15 shows an inverse square and inverse exponential relation between light output and SD separation, so it is not a surprise to get this output – SD distance relation in Figure 4.3 (top). SD pair with 4 cm separation detects significantly less light than 1 cm.

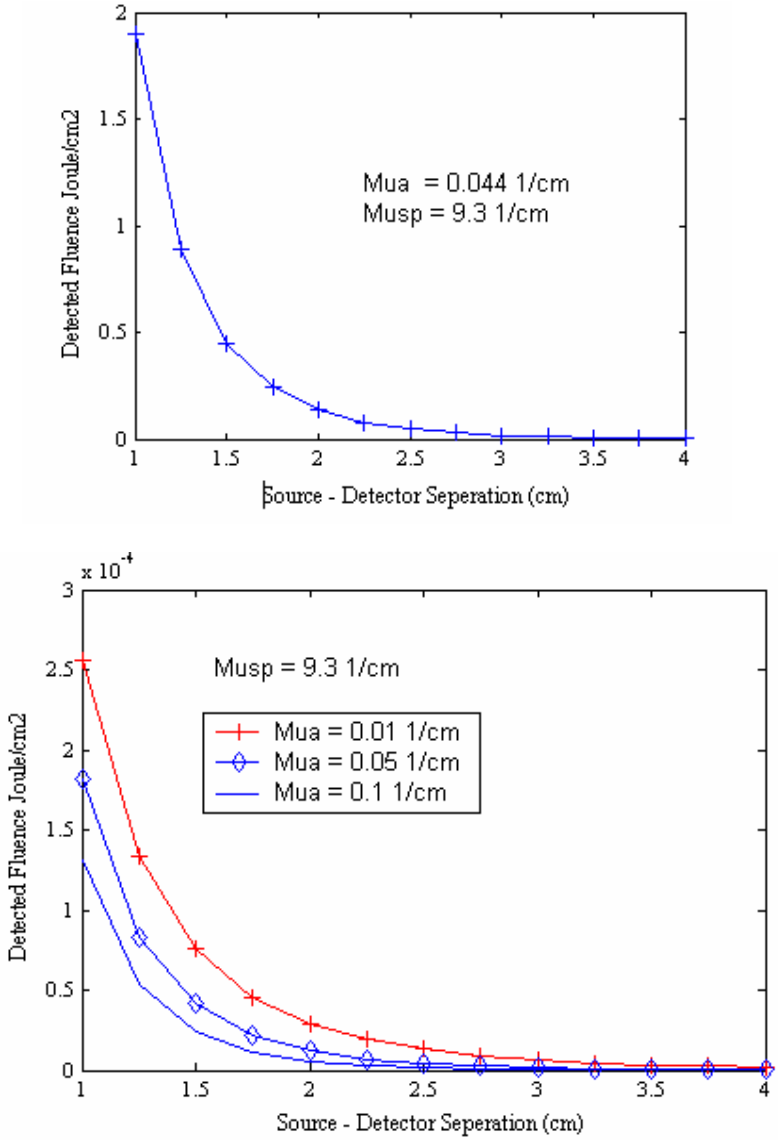

Figure 4.3 Light output decreases exponentially by increasing SD distance (top). For higher μ_a values exponential decay of output for increasing SD separation is deeper (bottom).

Figure 4.3 (bottom) summarizes dependence of the detected fluence to medium's optical properties. As we increase absorption, keep scattering constant, detected fluence decrease *in a different manner* for each SD pair. Since mean light path increases with SD distance light output decreases significantly and it becomes harder to see the effects of μ_a changes. In Figure 4.4 incident light intensity Io is increased for μ_a = 0.05 (1/cm) and μ_a = 0.1 (1/cm) such that the detected fluence at SD1 give the same fluence value as μ_a= 0.01 (1/cm). The lines in Figure 4.4 differ because of the nonlinear effect of μ_a on fluence measurements as in Eq 2.12-2.15.

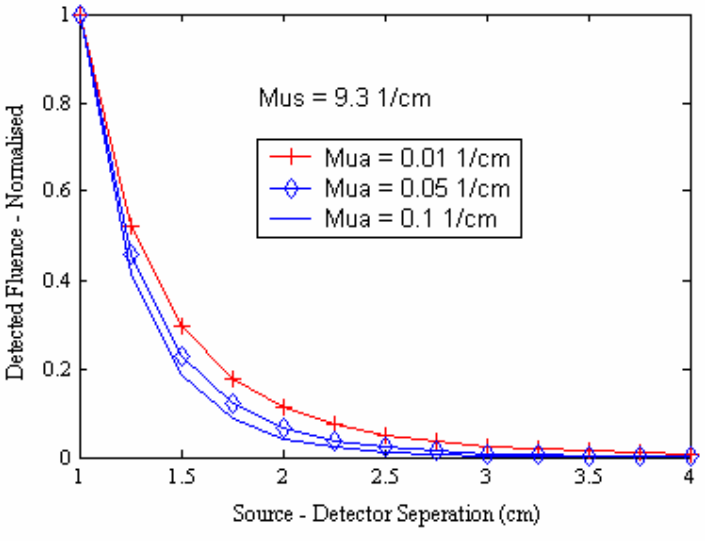

Figure 4.4 Effect of absorption coefficient on detected fluence values are normalized with respect to their values at source – detector separation 1 cm.

Medium optical properties are determined by μ_a and μ_s‘. An exponential relation between output and μ_a‘ is seen in Figure 4.5. How does the relation between μ_a and μ_a‘ affect output? Figure 4.6 can guide us in interpretation.

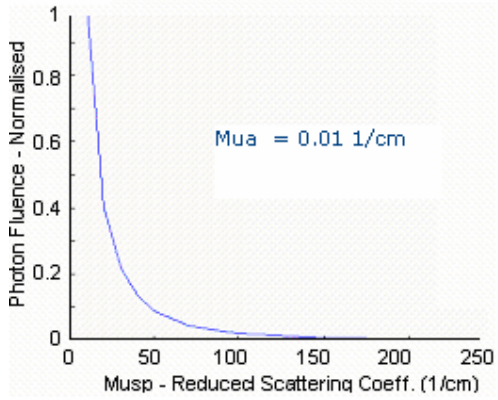

Figure 4.5 Exponential decrease in output for increase in scattering coefficient at SD2 (2 cm).

Again an increase in μ_a causes an exponential decrease in output figure 4.6. Data presented is for both 9 and 100 1/cm background.

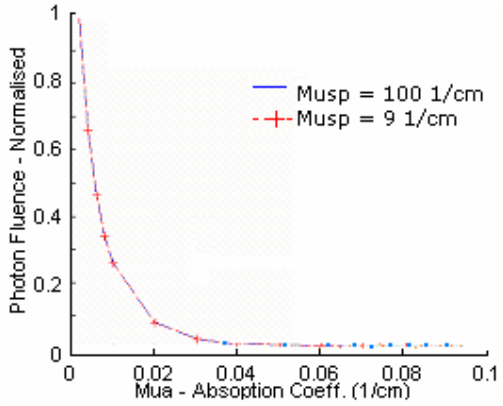

Figure 4.6 Normalized data for increasing absorption constant with μ_s‘ = 9 and 100 1/cm, SD2 (2 cm).

In Figure 4.6 data for different μ_s‘ values fit, demonstrating the non – linear relation of μ_a and μ_s‘. This is proving $\kappa \approx \sqrt{3\mu_a\mu_s'}$ relation from Eq. 11,12 for highly scattering media.

4.1.2 Perturbations with Constant Power

Depth of the homogenous medium is decreased by adding an absorbing layer with increasing height. We were expecting the core of the photon distribution to be around z ≈ SD/2 (Eq. 2.13), and a significant change around z ≈ SD.

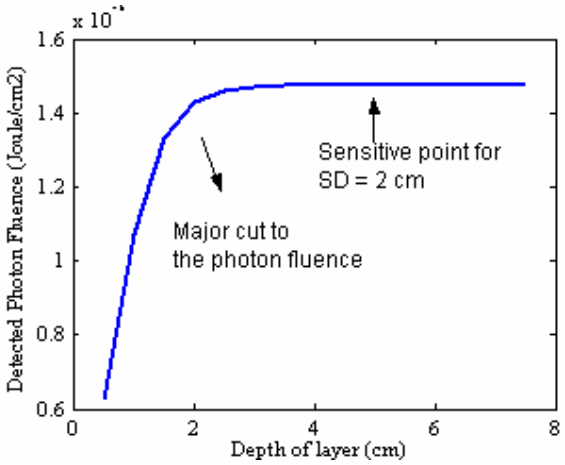

Figure 4.7 Change of output for SD2 by depth from the surface of medium at 0.1 Watt.

In Figure 4.7 it can be seen that mean path of diffuse photons, reaches 2 cm below from the surface. However, a perturbation up to 5 cm below the surface can be detected although change of output is infinitesimal. SD2 and SD3 difference for sensitivity and

photon migration depth is revealed in Figure 4.8. By increasing SD distance we shifted photon density downwards and were able detect a perturbation at 5.5 cm. Photon density reached 3 cm below the surface which shows itself with a sharp decrease of output due to layer perturbation.

Sensitivity of a detector to a point 5 cm below the surface is something that can be easily detected with numerical modelling. In real life the very small percentage of photons that reach deeper and bring information are hard to detect. Can we enhance this small percentage, which does not belong to the main stream of banana pattern, and probe deeper?

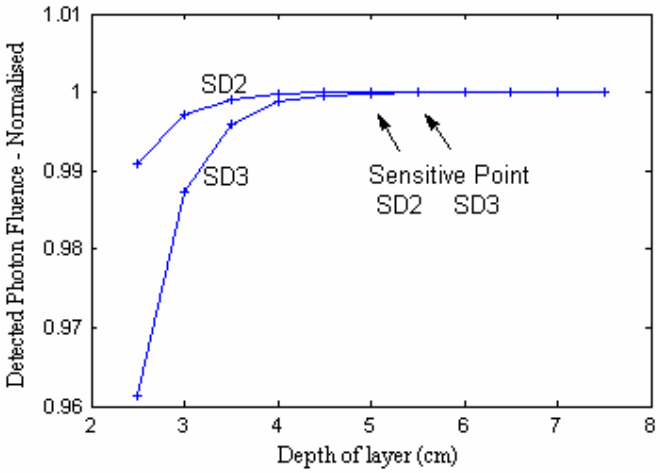

Figure 4.8 SD2 and SD3 difference in probing deep for 0.1 Watt and 1 Watt input power.

If we increase the power of incident light, number of photons that diffuse in the medium will automatically increase and more photons will probe deeper structures. In Figure 4.8 incident light power is increased ten times, as a result photons that probe deep layer may increase but their percentage in over all distribution does not seem to change. To evaluate this we take a closer look at the data and evaluate the data for 1 mm^3 voxels. SD2 detection which was sensitive above 4.4 cm for 1Watt incident light power, become sensitive to 5.1 cm deep at 5 Watt. A piece of data is shown below, for a complete set of data please refer to Table G.3.

Table 4.1
Raw PMI data showing an increase in sensitivity for higher power input.

Depth of medium (cm)	SD2 Detected Photon Fluence (Joule/cm2)		
	1 Watt	3 Watt	5 Watt
4.9	1.3455e-005	4.0365e-005	6.7276e-005
5	1.3455e-005	4.0366e-005	6.7276e-005
5.1	1.3455e-005	4.0366e-005	6.7276e-005
5.2	1.3455e-005	4.0366e-005	6.7277e-005

It has to be noted that PMI too will not see this difference for higher SD separations where output and sensitivity decrease significantly.

4.1.3 Power and Perturbations

We have seen that for a homogenous medium output – power relation was linear with slopes values inversely proportional to SD distance, because of the increase in pathlength. How will a perturbation contribute to this decrement? It is expected that because of the fact that SD3 has its main photon stream deeper than SD2 a perturbation will disturb the output of SD3 more than SD2. We investigated the change in outputs of SD2 and SD3 with respect to depth of the layer and power of incident light, in the range 15 mm below the surface where is the most sensitive place for both SD2 and SD3.

Table 4.2
Slopes of incident light power versus detected fluence data

Medium Depth	1 Raw slopes between 0.1 - 0.2 Watt		2 Normalised for medium heights		3 Normalised for SD separation	
	SD2	**SD3**	**SD2**	**SD3**	**SD2**	**SD3**
75 mm	$1.4749\ 10^{-5}$	$2.0149\ 10^{-6}$	1	0.13662	1	1
15 mm	$1.3334\ 10^{-5}$	$1.444\ 10^{-6}$	1	0.10829	0.90408	0.71662
10 mm	$1.0744\ 10^{-5}$	$0.86308\ 10^{-6}$	1	0.080332	0.72848	0.42834
5 mm	$0.6205\ 10^{-5}$	$0.34317\ 10^{-6}$	1	0.055302	0.42075	0.17031

Figure 4.9 - 4.10 presents data taken for SD2 and SD3 for 75, 15, 10, and 5 mm deep medium. There is a linear relation between detected fluence and incident light power. Slopes of the data are summarized in Table 4.2. From the second data set of Table 4.2 it can be seen that for homogenous case SD3 output is 7.3 times lower than SD2 output. For different perturbations – homogenous medium depths, relative outputs for SD2 and SD3 are significantly different. A perturbation 5 mm below the surface causes output ratio of SD2 and SD3 change to 18 from 7.3.

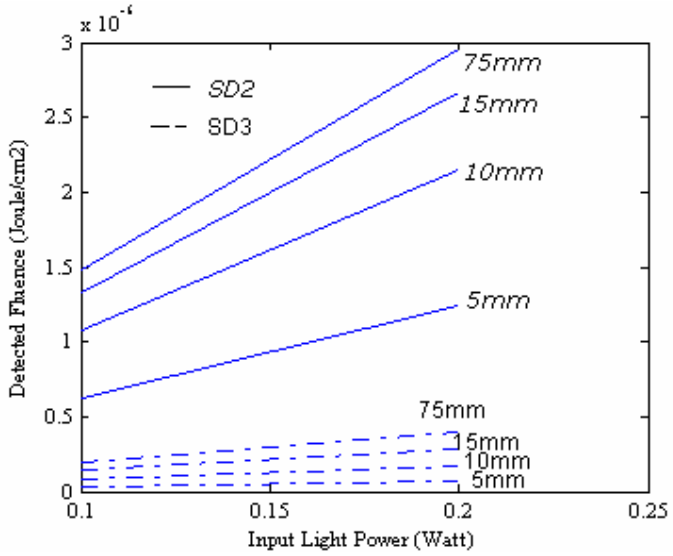

Figure 4.9 Increase of outputs of SD2 and SD3 pairs at higher input power, no – perturbation, and perturbation – 15, 10, 5 mm deep medium case.

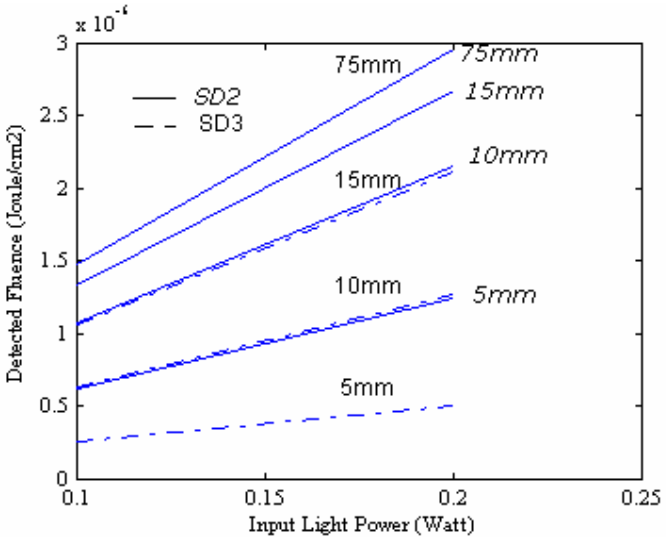

Figure 4.10 Increase of outputs of SD2 and SD3 pairs at higher input power, no – perturbation, and perturbation – 15, 10, 5 mm deep medium case - normalised for SD2, displaying relative change ofSD2 and SD3.

Data set three of Table 4.2 demonstrates how the depth of photon migration differs for different SD pairs. A medium 15 mm deep is covering 90% of the diffuse photons for SD2 pair, however perturbation below 15 mm deep medium cuts 29% of diffuse photons of SD3.

Data set two Table 4.2 is presented in Figure 4.11 in a similar manner to Figure 4.3.

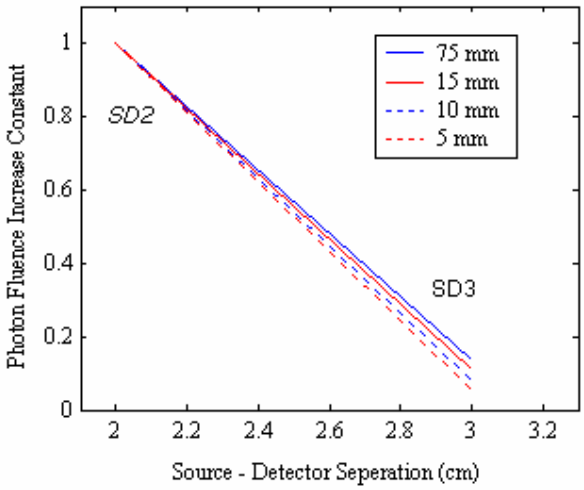

Figure 4.11 Table 4.2 data set two data showing decrease of SD3 output relative to SD2 output in case of a decrement in medium depth due to a perturbation

Relative slopes of SD2 and SD3 are different enough to reveal the depth of the perturbation at 15, 10 and 5 mm. However it has to be reminded that taking slopes does not give us extra information, because 10 times increase in input power leads 10 times increase in output at every SD distance. Because of that taking slopes and taking data at constant power gives the same results for now. Perhaps in the future there may be tools to detect that change in the order of 10^{-4} with power and taking slopes will give more information.

When we do real measurements we will measure output at different SD pairs and since the optical properties of the medium will be unknown and SD2 and SD3 ratio will be unknown, its hard to say whether there is a perturbation or not, or the depth of a perturbation from the decrease of SD3 output. If we find a medium where SD2 and SD3 slopes are equal or known for no perturbation case we might have a chance to speculate about the depth of the layer. We will come back to this issue later.

4.2 Experiments

4.2.1 Homogenous medium

Figure 4.12 shows a linear relationship between number of incident photons and measured diffuse fluence.

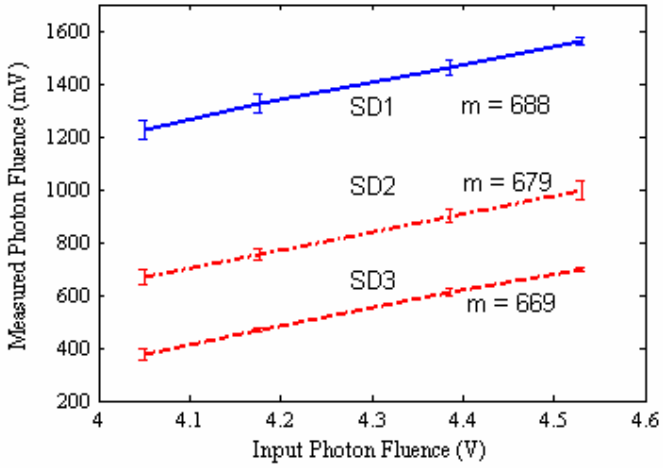

Figure 4.12 Source – detector (SD) pair with 1 cm distance (SD1), with 2 cm distance (SD2) and with 3 cm distance (SD3) outputs for increasing input power.

Output difference between SD1 and SD2 is higher than difference between SD2 and SD3. This underlines the exponential decrease of output with SD separation in figure no. Taking into account the amplifier circuit (10 times), the measured fluence is 1/40 of incident fluence for SD1. Although they look almost parallel there is a difference in slopes of SD1, SD2 and SD3, which is because of the variation of their mean optical paths. To investigate their optical pathlengths calculating their attenuation 'A' will be useful (Eq. 4.1).

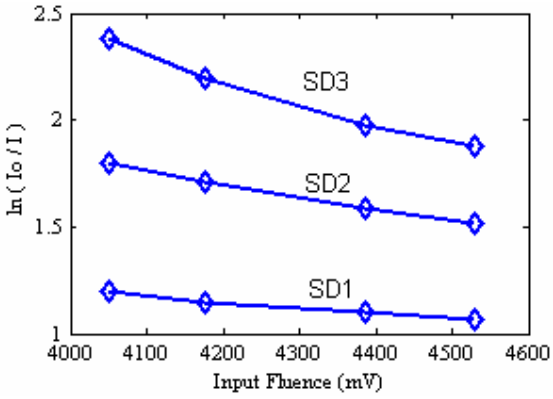

Figure 4.13 Attenuation of light for SD pairs.

Figure 4.13 shows how optical pathlength increase with SD separation indirectly; for input power 4530 (mV) attenuation for SD3 is around 1.8, for SD2 1.5 and for SD1 1. Lines are expected to be constant and parallel because magnitude of input power does not affect the pathlength but the density. However it can be said that for higher power input

they are diverging to constant numbers around 1 – 2. The exponential like drop seen in SD2 and SD3 results may be due to an error in detection sensitivity. Oscilloscope is more sensitive to changes in higher values and especially SD3 measurements can be a victim of this. Also amplifier circuit may exaggerate SD1 data more than other pair's data. It is clear that line for SD1 is the one closer to a constant value. Its shift for lower input powers is probably due to the lasers performance at 63 mA because the best range to work with our laser is between 70 and 80 mA. Figure 4.13 is similar to Figure 4.2 in the way that an SD3 and SD2 difference is lower than SD2 and SD1 difference.

4.2.2 Perturbations and Power

Inserting screen into the tank disturbs the system and effects measurements. Among all measurements, data taken with position adjuster have been the most consistent. Even this system is open to many noise sources. 5.5 cm screen was moved upwards for positions 15, 10, 5 mm and data were taken for four input powers, at 63, 65, 70, 75 mA diode currents (Figure 4.14) (Table 4.3). SD2 and SD3 stands for source – detector pairs at 2 cm and 3 cm distance respectively.

Table 4.3
Slopes of incident light power versus detected fluence data

Medium Depth (mm)	1 Raw slopes between 0.23 – 0.44 mW				2 Normalised for medium heights		3 Normalised for SD separation	
	SD2	**R^2**	**SD3**	**R^2**	**SD2**	**SD3**	**SD2**	**SD3**
75	679.16	0.9999	669.93	0.9987	1	0.98641	1	1
15	679.82	0.9987	564.58	0.9977	1	0.83049	1.001	0.84275
10	662.01	0.9994	533.62	0.9933	1	0.80606	0.97475	0.79653
5	623.68	0.9994	173.61	1	1	0.2776	0.9183	0.2585

Significant decrease in output and slope for both SD2 and SD3 is seen in Table 4.3 data set one and Figure 4.14 as the depth of homogenous medium decreases. Because of the high (≈ infinite) absorption constant of the metal screen all photons that are scattered from deep tank and near to surface that strike the screen are absorbed. Still there is a high variability of the places that photons travel and reach the detector because of the high concentration of scattering particles and scattering probability (10 scatters in 1 cm depth).

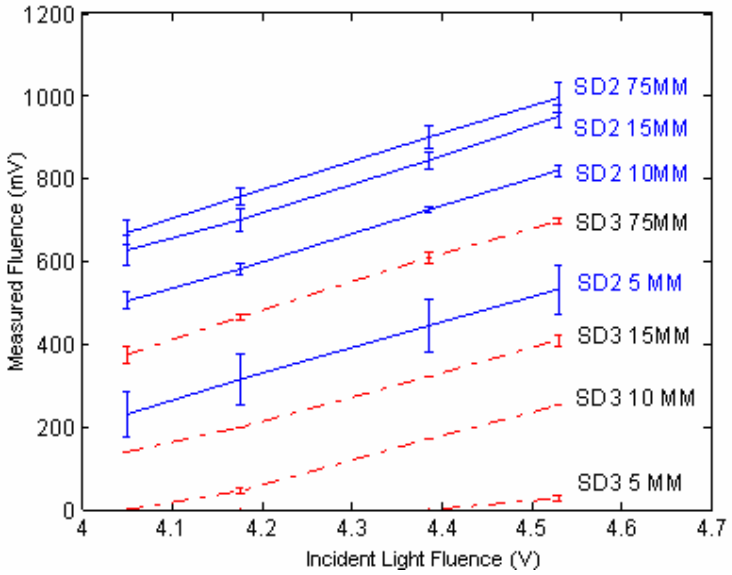

Figure 4.14 Increase of output for increasing incident light power.

Table 4.3 data set two shows relative changes of SD2 and SD3 at different depths. It is close to unity, 0.98 for 75 mm while it decreases to 0.80 in the presence of the absorber 10 mm below the surface. 10 mm below the surface is approximately where the main stream of the diffuse photons lie. For a screen 5 mm below the surface since most of the diffuse photons that SD3 detect are cut but still SD2 have room, relativity is huge (table no data set one-two).Data set three again displays how the depth of medium affects the output for SD2 and SD3 differently.

A linear relation of output and input can be seen in Figure 4.14. Application of a perturbation disturbs the homogenous medium and alters the measured fluence but this alteration is not related to photon density again. Even with inhomogeneities if we increase input 10 times we expect a 10-fold increase in output. Large error bar for SD2 at 5 mm may be due to an unnoticed change in the system during measurements. Table no data set three is normalized with SD2 data and displayed in Figure 4.15.

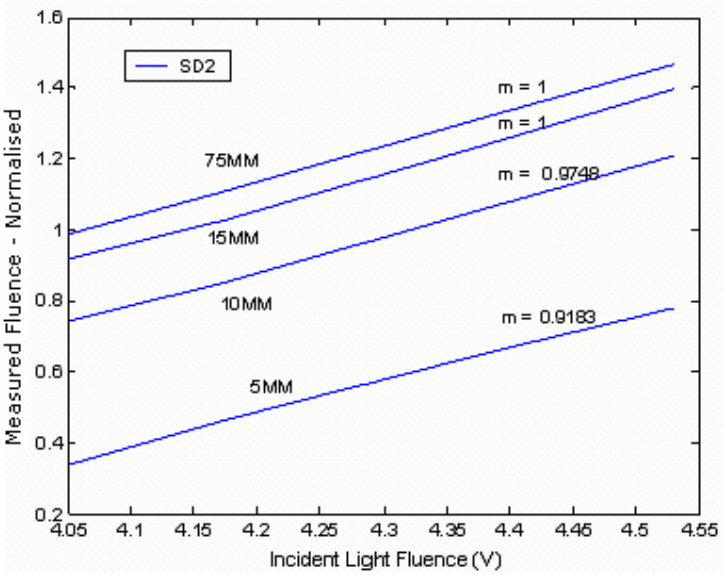

Figure 4.15 Normalized output data of SD2 with screen perturbations

As the perturbations are applied for every 5 mm the output decrease was more than before but consistent with Figure 4.9 implying the curve of banana (Figure 4.15). It is like cutting strips of equal width from a half disk; each strip has equal widths but as we head to the diameter of the semi-disk the area of the cuts increase.

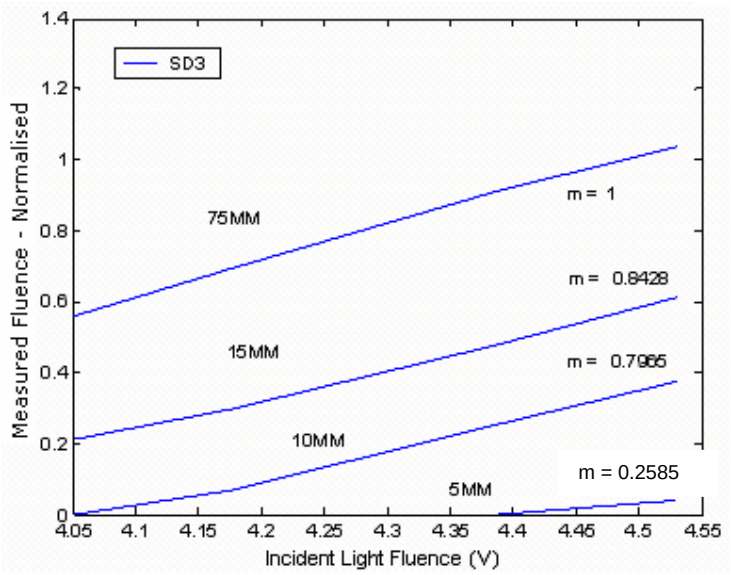

Figure 4.16 Normalized output data of SD2 with screen perturbations

Table 4.3 data set two is displayed in Figure 4.17. SD2 and SD3 slopes are equal or nearly same for homogenous non-perturbed case, relative slopes reveal the place of an inhomogeneity (Figure 4.17).

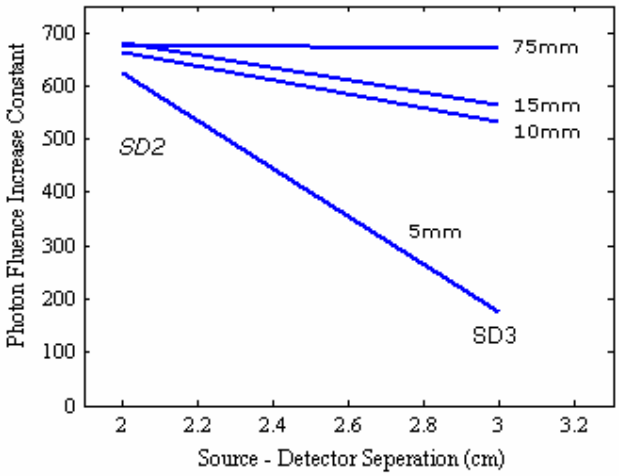

Figure 4.17 Decrease of SD3 output relative to SD2 output in case of a decrement in medium depth due to a perturbation (Table 4.3 data set two).

Figure 4.17 and Figure 4.11 were expected to be similar but experimental data showed a better display of disturbance due to a perturbation. Especially at 5 mm there is a significant drop in SD3 slope. Also by the simulations we could not get such close slope values of SD2 and SD3 at 75mm(no perturbation case). Experimentally, SD2 measurement is only two times bigger than SD3 and slopes are very close (98%). For comparison purposes we normalized experimental and simulation data, two times (Figure 4.18).

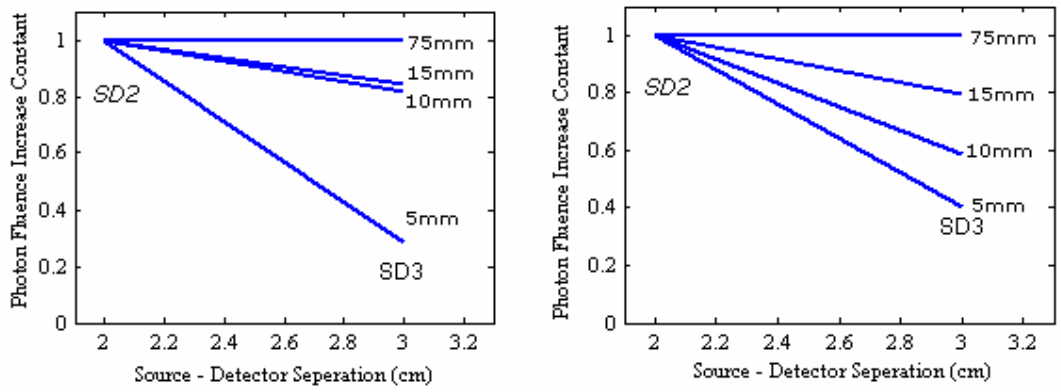

Figure 4.18 Figure 4.17 (left) and Figure 4.11 (right) normalized; decrease of SD3 output relative to SD2 output, experimental results (Table 4.3 data set two – normalized) (left) and simulation results (Table 4.2 data set two – normalized) (right).

4.2.3 Perturbation with constant power

Depth of the homogenous medium is decreased from 75 mm to zero by moving screen upwards at 5mm steps for SD2 (2 cm separation). In Figure 4.19 it can be seen that

banana pattern of photon density for SD2, reaches 15 – 20 mm below the surface. However our sensitivity to see an inhomogeneity at 20 mm is still low.

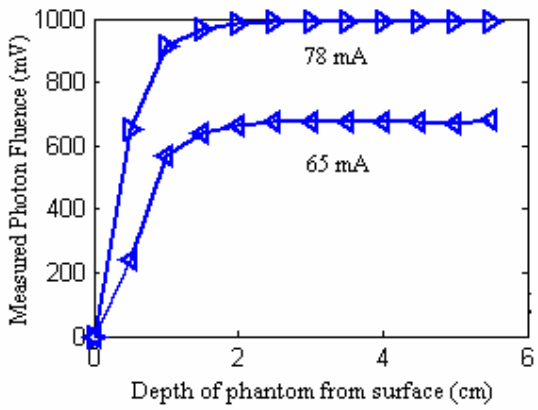

Figure 4.19 Change of output for SD2 by depth of medium at 65 and 78 mA.

With 65 mA laser diode current, systems sensitivity starts at 25 mm. Existence of screen causes small changes in output starting from 25 mm but information is dominated with system noise. At 15 mm we can see 20 mV decreases in output. Will increasing the input power enhance our sensitivity? Taking the same measurements for 78 mA laser diode current a significant decrease (20 mV) is observed again for 15 mm depth (Figure 4.19).

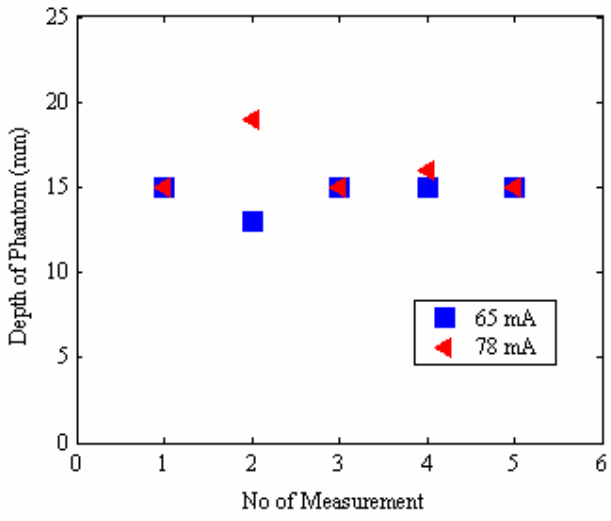

Figure 4.20 Ten measurements, five with 65 mA and five with 78 mA made showing their sensitivity starting at 15 mm depth, with the tendencies of upwards and downwards respectively.

However, increasing the diode current cause the output power at the end of the input fiber rise from approximately 0.23 to 0.50 (mW), which may cause a difference only

in millimeters scale (Table 4.4). So that concentrating on 15 mm deep region measurements are made (Table 4.4). Figure 4.20 we observed a sensitivity starting from 15 mm. Two of five measurements with 78 mA display a change in output deeper that 15 mm, while one of the measurements with 65 mA below 15 mm. This result intuitively makes us think that increasing power enhances sensitivity. A more powerful laser and more sensitive tools should be used for better results.

Table 4.4
Data of ten measurements showing starting points of sensitivity for 65 mA and 78 mA

<table>
<tr><td></td><td>Depth of phantom mm)</td><td colspan="5">Measured Fluence from SD2 at 78 mA (mV)</td><td colspan="5">Measured Fluence from SD2 at 65 mA (mV)</td></tr>
<tr><td rowspan="5">Primitive Sensitive region</td><td>25</td><td>1010</td><td>940</td><td>940</td><td>950</td><td>947</td><td>640</td><td>670</td><td>640</td><td>647</td><td>740</td></tr>
<tr><td>19</td><td rowspan="3">≈1010</td><td rowspan="4">920</td><td rowspan="3">≈940</td><td rowspan="2">≈950</td><td rowspan="3">≈947</td><td rowspan="3">≈640</td><td rowspan="4">≈670</td><td rowspan="3">≈640</td><td rowspan="3">≈647</td><td rowspan="3">≈740</td></tr>
<tr><td>18</td></tr>
<tr><td>17</td></tr>
<tr><td>16</td><td rowspan="2">920</td></tr>
<tr><td rowspan="3">Sensitivity starts</td><td>15</td><td rowspan="3">984</td><td rowspan="3">920</td><td rowspan="3">920</td><td rowspan="3">620</td><td rowspan="3">620</td><td rowspan="3">630</td><td rowspan="3">720</td></tr>
<tr><td>14</td></tr>
<tr><td>13</td><td>650</td></tr>
</table>

Primitive sensitive region means that the output has tendency to change but is dominated by noise, which starts 25 mm below the surface (Table 4.4).

4.3 Sources of Error

4.3.1 Systematic noise

There is ±100 mV systematic noise with zero mean and (low frequency) baseline drift ±10 mV that can be read on the oscilloscope. Frequencies that contribute to noise can easily be seen by Fast Fourier Transform (FFT); for the FFT display of our signal please refer to Appendix. Other possible sources of noise may be:

1. Circuit elements may cause noise due to increase of temperature by time (resistances, amplifier, and filter); power supply instabilities.

2. Diode laser does not have a temperature regulator (*Cooled Laser Diode Mounts*). With a temperature controller the laser current or the optical output

power and the temperature of the laser diode can be precisely regulated. Thus laser diode works as a stable optical transmitter.

3. Laser Driver LDC500 is an older model and delivers 500mA, would be hard to regulate 5mA, we may be missing sensitivity. Running the laser at a constant current and attenuate it would be a solution but the power of the output would decrease.

4. Intralipids optical properties may change by time.

5. Changing fibers positions as the procedure and loss of contact with intralipid; change of the level of intralipid filling the tank; any unnoticed change of set – up during experimentation.

6. Oscilloscopes sensitivity is our reference for especially SD3. Its less sensitivity for smaller values and the fact that we amplify the signal 10 times, may lead to errors.

7. Any error characteristic to the operation of a part of the system (Active area of the photodiode etc.).

4.3.2 Random Noise

- Although experiments are done in dark environment background electromagnetic radiation.
- Electromagnetic interference to circuit; UPS, inefficient grounding, operating devices in the laboratory (computers etc.), NMRS in the neighbor laboratory.
- Light scattering noise; photons strike the detector randomly. This is probably the main reason for ±10mV baseline drift.

5. DISCUSSION

The simulation and experimental results demonstrate that the only thing that changes with intensity of light is the amount of diffuse photons.

Similarly both results showed a difference of mean photon pathlengths for different source detector separations.

PMI and experimental results differ in the way that output fluence differs for homogenous case between SD2 and SD3. PMI results in a 7.3 fold decrease while experiments two fold (Table G.1-G.2). PMI uses diffusion approximation to RTE so Eq. 2.15 yields same decrement, we tried electrostatic analogy:

$$E = \frac{1}{4\pi\varepsilon_0}\frac{p}{(a^2 + r^2)^{3/2}} \tag{5.1}$$

With dipole separation 2a we will select the electric field line r = a assuming that this electric field line resembles the core of the 'banana' and ends up almost normal to the negative charge (Figure 2.7-2.8). Then we calculate electric field, E for different dipole separations (SD distance 2 and 3 cm) and take ratio:

$$E = \frac{1}{4\pi\varepsilon_0}\frac{q2a}{(a^2 + a^2)^{3/2}} = \frac{1}{4\pi\varepsilon_0}\frac{q2a}{2^{3/2}a^3} = \frac{1}{4\pi\varepsilon_0}\frac{q}{\sqrt{2}a^2} \tag{5.2}$$

$$\frac{E_1}{E_2} = \frac{a_2^2}{a_1^2} = \frac{3^2}{2^2} \approx 2 \tag{5.3}$$

Electrostatic analogy describes the decrease in output due to SD distance better than diffusion approximation.

Secondly we comment on Figure 4.17 – 4.11. To use SD differences as a tool for detection of a layer or perturbation, optical properties of the medium should be known. This is impossible for medical detection. However in the low absorption limit $\kappa r << 1$, depth of diffuse photons does not depend on optical properties (Eq. 2.13). We calculated this for our phantom:

$$\kappa \equiv \sqrt{3\mu_a\mu_s'} = 1.05 \qquad \kappa r \approx 2 \tag{5.4}$$

κr is neither smaller than one nor very bigger. This is same for tissue optical properties so that is not applicable. However experimental output gives promising results more studies have to be done. Especially as will be mentioned in future works, solid phantoms in which an inclusion will be embedded may give better results.

Finally, experimentally and computationally we would like to comment on results for enhancement of sensitivity with increasing power as seen in Fig. 4.20. We observed this for PMI (not for every case increasing ten times do not effect while increasing three, five times effect etc.). Experimental results suffer form severe electromagnetic interference noise. The improvement in sensitivity may be the result of an increase in density of diffuse photons and photons that probe deeper and bring information. Generally the photon density increase homogenously, means the percentage of the small portion of photons (not the core) that probe deeper does not change theoretically and experimentally (for now). So the signal coming from the photons of the core expected to dominate the signal again and probability of our sensing is still low and restricted with the tools' (fibers-photodiode-oscilloscope) sensitivity.

PMI toolbox uses diffusion approximation to RTE. Diffusion approximation solves the problem only for homogenous medium, of course then perturbations effect is added. PMI gives error for a thin slab (depth =<10 mm) and exaggerates the decrement of output fluence for increasing SD distance. It definitely fails near boundaries and for any case that does not satisfy $\mu_a << \mu_s'$, but can be regarded as successful in describing light propagation in turbid media.

6. CONCLUSION

Diffuse optical tomography (DOT) and near infrared spectroscopy (NIRS) are techniques that suffer from uncertainty of light path and probing depth inside the tissues. We have investigated the hypothesis that probing depth with continuous wave, coherent infrared light in human tissue is a function of the incident light power and source-detector distance. The hypothesis is tested both numerically by the help of a Photon Migration Imaging (PMI) Toolbox (finite-element model diffusion approximation to the radiative transfer equation) and experimentally.

Changing intensity of light changes the amount of diffuse light but does not affect the mean path of photons. If light could go deeper as we increase the light intensity we would probe deeper.

We were searching for a way to find an inhomogeneity independent of μ_a and μ_s'. If we could find a difference in increase of output for two SD pairs, this could be used. However for any medium and for any SD distance light propagation is directly proportional to incident light, an increase of ten times would produce and increase in output ten times for any medium at any SD distance.

However our experimental results are promising and reveal existence of an inhomogeneity. More work should be done.

6.1 Future Work

This study can be followed by measurements with solid phantoms which will have less error due to the medium. Solid phantoms can be made from gelatine and intralipid and may give more consistent results. Further step would be the preparation of phantoms with different optical properties. This can be done by adding absorbers such as Indian ink.

More importantly the experimental set up should be enhanced:

- A cooled laser mount would regulate the output and works as a stable optical transmitter.

- The filter and amplifier should be suitable for this purpose and should eliminate unwanted frequencies successfully and decrease noise level. The circuit should be robust and mounted in a metal cover to eliminate electromagnetic interference.
- Our fiber is most commonly used with 650 or 660 nm because of its relatively low attenuation at that wavelength. 850 nm light will not go very far (15-25 m). Fibers should be selected suitable to the wavelength of laser and should be kept short.
- The environment should be protected from electrical interferences.

Interaction of light and tissue is a very interesting subject; further studies would be modelling of light propagation in inhomogeneous medium, the effect of electric field to the optical properties (it is known that scattering constant of nerve cells change by applied voltage). Studies on semi – infinite geometry is useful for mole cancer detection and quantization, which shows itself with an increase of absorption constant and depth.

APPENDIX A
PMI TOOLBOX

A.1 Overview of PMI Toolbox

The Photon Migration Imaging (PMI) Toolbox implements numerous algorithms for performing the forward and inverse calculations associated with diffusive optical imaging. Some of the features supported by the PMI Toolbox include:

- Infinite, semi-infinite, and infinite-slab geometries
- Homogeneous and inhomogeneous media
- Simulation routines for modelling DOT experiments
- Fitting data for background optical properties
- Time-domain and frequency-domain imaging
- Interfaces with Monte Carlo and finite difference forward solvers
- Linear and non-linear image reconstruction
- 2-D data visualization and 3-D volume visualization
- Data calibration

A.1.1 Using the PMI Toolbox

The PMI Toolbox runs under Matlab, which supplies many of the supporting routines used by the toolbox. While most routines will run without any toolboxes outside the core Matlab package, a small number of routines use functions from other Matlab toolboxes. In particular, some of the routines for fitting background optical properties use routines from the optimization toolbox (sold by Mathworks as a separate package). To use the PMI Toolbox, the user first sets up a pair of structures, traditionally called SD and Medium. These structures can either be generated by hand or extracted from the data file (if the data is stored using the PMI data format). Having generated the SD and Medium structures, the PMI Toolbox provides standard routines for calculating the forward problem, inverting the data or (for simulations) generating the data, and then visualizing the results.

A.1.2 Solution to Forward Problem

1) Uniform Optical Properties

In the case of media with spatially uniform optical properties, the method is:

pmi.Fwd.Method.Type = 'Helmholtz Homogeneous';

This finds the analytic solution to the Helmholtz equation for the given geometry.

2) Linear Methods for Non-Uniform Optical Properties

The First Born approximation is specified by:

pmi.Fwd.Method.Type = 'Born';

The Rytov approximation is specified by:

pmi.Fwd.Method.Type = 'Rytov';

This approach neglects secondary scattering effects, takes into account only first scatter.

1- The first Born approximation,

$\Phi = \Phi o + \Phi pert$

2- The Rytov approximation,

$\Phi = \Phi o.\exp(\Phi pert)$

3) Non-Linear Methods for Non-Uniform Optical Properties

The N*th*-Born approximation is specified by, where *n* is the order of the approximation:

pmi.Fwd.Method.Type = 'BornN';

This method gives solution for multi scattering photons.

Table A.1
Important structures of PMI Toolbox

<table>
<tr><td>genBornData()</td><td>Calculate total fluence.</td></tr>
<tr><td colspan="2">For all other methods, an empty list is returned. Given a previously solved forward problem (using genBornMat(), for example), genBornData() calculates the total field given a (possibly empty) set of perturbations in Medium.Object{:}.

<table>
<tr><td rowspan="2">Outputs:</td><td>Phi</td><td>The total fluence</td></tr>
<tr><td>Phi2pt</td><td>Total fluence at each voxel (FullBorn methods only)</td></tr>
</table>

If Method is "FullBorn", then in addition to the total fluence, genBornData() returns the fluence at every voxel throughout the volume Phi2pt.</td></tr>
<tr><td>Medium. Object</td><td>A vector of cells that contain structures defining perturbations to the optical properties.</td></tr>
<tr><td colspan="2">Every structure contains a field Medium.Object{}.Type that specifies what kind of perturbation it describes. The legal values for Type are "sphere", "block", and "image". Given a (possibly empty) list of perturbations stored in Medium.Object, genBornData() calculates the total perturbed fluence.</td></tr>
<tr><td>Medium.CompVol</td><td>A structure that declares the volume being imaged.</td></tr>
<tr><td colspan="2">X, Y, and Z must contain regularly-spaced intervals. The toolbox is not smart enough to detect non-uniform grids for you. If non-uniform grids are absolutely essential, Medium.CompVol.Type can be set to "list". Now, Medium.CompVol.X, Medium.CompVol.Y, and Medium.CompVol.Z are vectors that directly specify the x y z location of every voxel and the vector Medium.CompVol.Volume gives the volume at every voxel (which need not be constant).</td></tr>
<tr><td>Medium.Geometry</td><td>A text string that defines the imaging geometry to be used</td></tr>
<tr><td colspan="2"></td></tr>
</table>

Currently supported values are 'infinite' (infinite medium, no boundaries), 'semi' (semi-infinite medium, boundary at z=0), and 'slab' (infinite slab, boundaries at z=0 and z=Z).

Medium.Muao is the optical absorption coefficient in 1/cm.
Medium.Muspo is the transport scattering coefficient in 1/cm.
Medium.idxRefr is the index of refraction.

The diffusion approximation breaks down for small scattering coefficient, so Medium.Muspo should be at least 1.0. While the diffusion approximation is valid, the infinite slab solution can fail to converge if the absorption coefficient is too small so small absorption coefficients should be avoided as well.

SD.Lambda	A vector of imaging wavelengths.

For fluorescence measurements, SD.Lambda contains both excitation and emission wavelengths and the measurement list is used to distinguish between the two processes. Wavelengths should be specified in nanometers.

SD.ModFreq; for frequency-domain imagers, the vector holds the source modulation frequencies, in Megahertz.

SD.SrcAmp *SD.DetAmp*	Matrices that hold the source amplitude and detector coupling coefficients respectively.

Because every measurement involves both a source and a detector, only the product SD.SrcAmp(iSrc,iWvl,iFrq)*SD.DetAmp(iDet,iWvl,iFrq) can be observed (for whatever iSrc, iDet, iFrq, iWvl is appropriate to a given measurement) and not the individual SD.SrcAmp and SD.DetAmp components (doubling all the SD.SrcAmp and halving all the SD.DetAmp leaves the final measurement unchanged). This indeterminacy is intrinsic to the forward problem. The product of the source and detector amplitudes has dimensions of Watts (detected fluence times the active area of the detector). When needed the source amplitude

matrix can be filled with different values and does not need to beuniform. The unit on the source amplitude is the power entering the tissues in Watts. This includes coupling effects. The detector amplitude is the aperture area [cm2] times the coupling coefficient for the detector, including the detector quantum efficiency.

For slab geometries *Medium.Slab_Thickness* specifies both the thickness of the slab and whether it lies above or below the z=0 plane (the tissue is located between z=0 and z=Z where Z is given by Medium.Slab_Thickness

A.2 Simple Code to Generate Data

```
% This code generates fluence data for source – detector separation 2 cm at 0.01W
% incident power for homogenous medium 10x10x7.5 cm^3 by 850 nm CW light.

doscat = 1;              % flags, 1 or 0
doabs  = 1;
thick  = 7.5;            % Slab thickness
Method = 'Rytov';        % Born or Rytov

% Generate SD structure with source/detector/measurement information

SD.Lambda  = [ 850 ];    % Define Wavelengths
SD.ModFreq = [  0  ];    % Modulation frequency; continuous wave

% Source and Detector Positions

SD.SrcPos = SetOptode( 5, 4., thick, 1);
SD.DetPos = SetOptode( 5, 6, thick, 1);

% Source and Detector Amplitudes;
```

```
SD.SrcAmp = 1e-2*ones(size(SD.SrcPos,1),                    % Incident power
                length(SD.Lambda), length(SD.ModFreq));
SD.DetAmp = 1e-3*ones(size(SD.DetPos,1), ...
                 length(SD.Lambda),length(SD.ModFreq));

% Generate a measurement list with all possible measurements

SD.MeasList = genMeasList(SD, 'all');
nWvl = length(SD.Lambda);

% Generate structure describing Medium to be imaged

Medium.idxRefr = [1.33];                                    % Optical Properties
Medium.Muao    = [0.044];
Medium.Muspo   = [9.3];
Medium.Geometry       = 'slab';
Medium.Slab_Thickness = thick;

% Volume to reconstruct

Medium.CompVol.Type  = 'computed';
Medium.CompVol.XStep = 0.5;
Medium.CompVol.X     = [0 10];
Medium.CompVol.YStep = 0.5;
Medium.CompVol.Y     = [0 10];
Medium.CompVol.ZStep = 0.5;
Medium.CompVol.Z     = [0.25 thick];              % Avoid the problematic z=0 case.
nVox = length(sampleVolume(Medium.CompVol));

% Generate forward matrix ('Born'/'Rytov' solve the homogeneous problem)

MeasList = SD.MeasList(:, :);
disp('Generating forward matrix - please wait');
```

```
[Phi0, A] = genBornMat(SD, Medium, MeasList, Method, [doabs doscat]);

% Define perturbations
% Define the layer with three times higher absorption constant

depth = 0;                                  %Homogenous case, there are no
perturbations
if (doabs)
  Medium.Object{1}.Type   = 'Block';
  Medium.Object{1}.Pos    = [ 5 5 depth/2];
  Medium.Object{1}.Dims = [10 10 depth];
  Medium.Object{1}.Mua    = 3*Medium.Muao;
  Medium.Object{1}.Musp   = Medium.Muspo;
end

% Generate perturbated data

Phi = genBornData(SD, Medium, MeasList, Method, Phi0, A, [doabs doscat]);
disp('Generating simulated data');
```

A.3 PMI Restrictions and Tips

- Optical constants are in units of 1/cm, source and detector positions and all relevant distances are in cm.
- PMI is not valid near air-tissue interface.
- There can be no light sources or detectors in the medium.
- Each voxel must have uniform X, Y, and Z dimensions and intervals must be regularly spaced.
- While the diffusion approximation is valid, the infinite slab solution can fail to converge if the absorption coefficient is too small so small absorption coefficients should be avoided.
- In slab geometry all fibers must be placed on the air-tissue (z=0 or z=Z) interface.
- It's possible to change both detector and source amplitudes.

- The unit of source and detector amplitude is power entering medium in Watts (fluence times the active area).
- Doubling the source amplitude and halving all the detector amplitude leaves the final measurement unchanged.
- A unit of detected fluence is Watts/cm2.

A.3.1 Restrictions due to Diffusion Approximation

- Medium must be homogenous; each particle is sufficiently isolated from each other, not in contact.
- Scattering by all particles is described by a single function (phase function).
- The diffusion approximation breaks down for small scattering coefficient, so μs should be at least 1.0.

APPENDIX B
PHOTOGRAPHS OF SET-UP

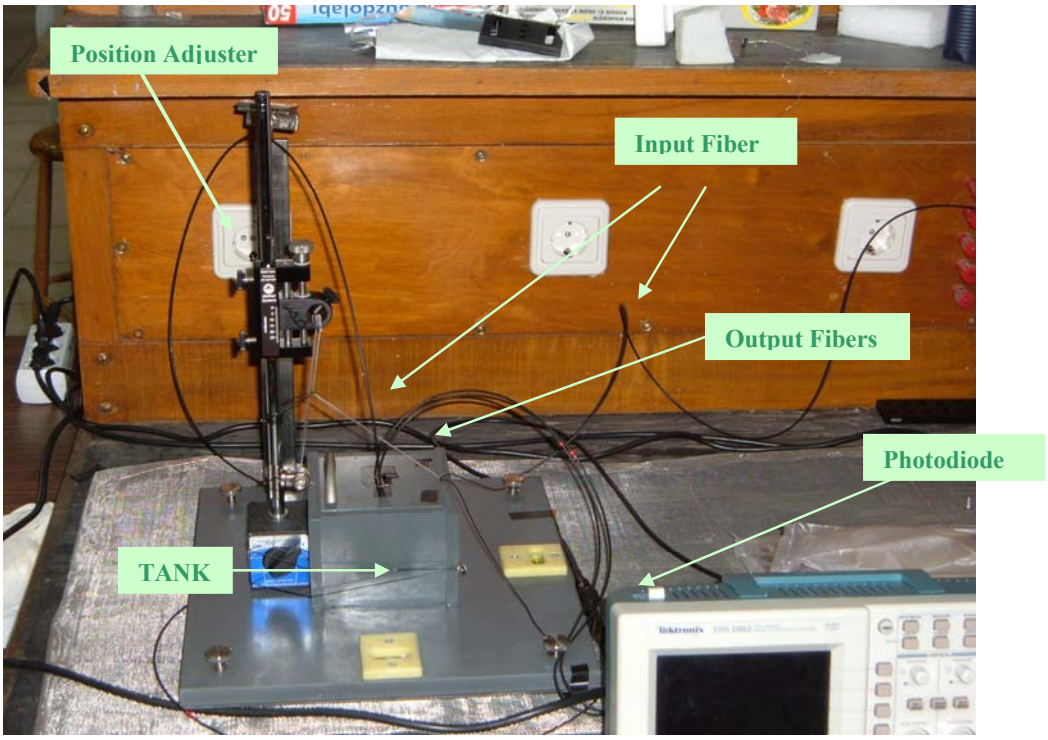

Figure B.1 Tank – position adjuster with input and output fibers

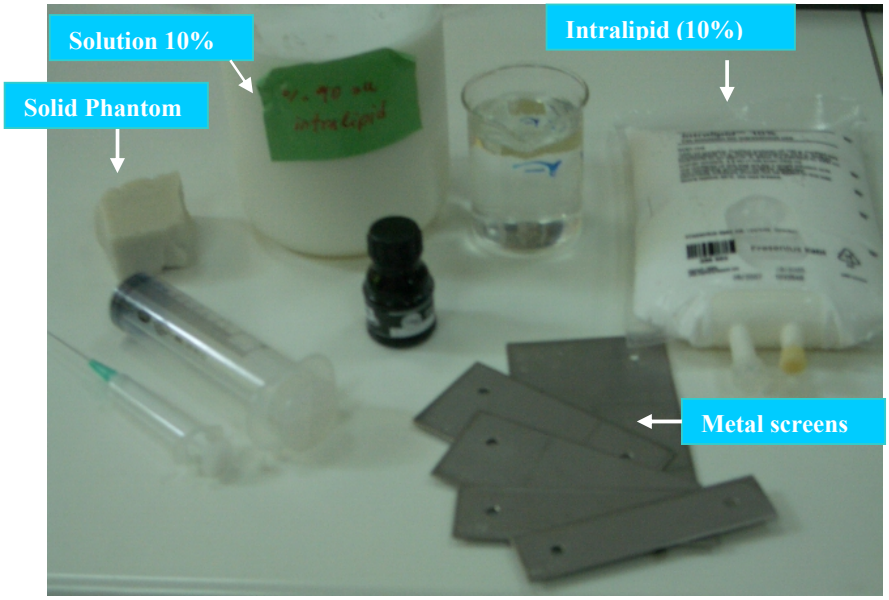

Figure B.2 Phantom

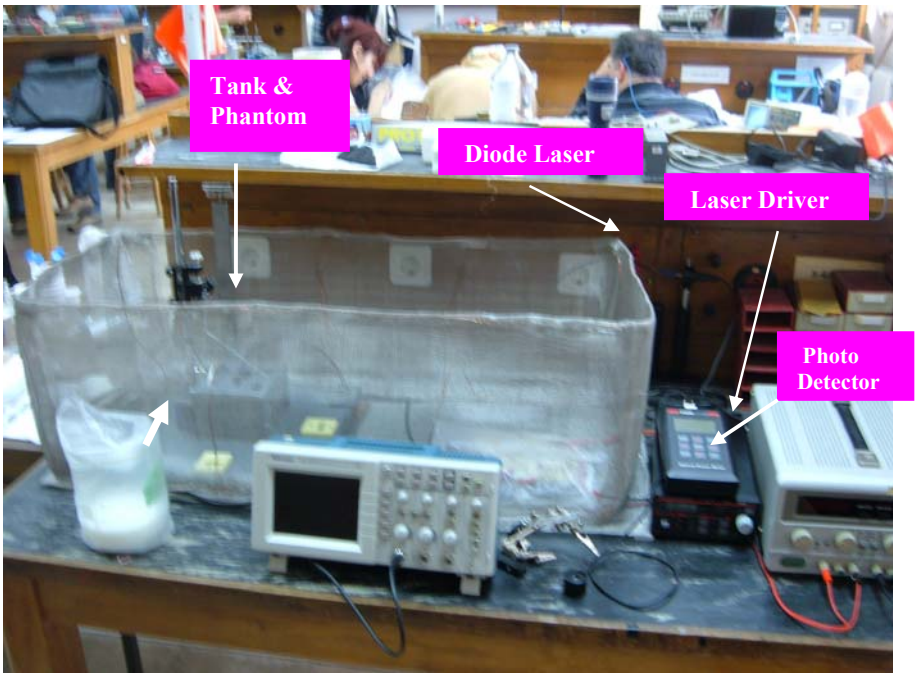

Figure B.3 General view of photon migration experiment set – up

APPENDIX C
ELEMENTS OF EXPERIMENTAL SET–UP

HDW100A Biopac Systems Force Transducer Tension Adjuster

The rugged design and stability of the mounting allow for fine position control.

Travel Range:	25mm
Resolution:	0.0025mm per degree rotation

SM05PD1A Thorlabs Mounted Silicon – Photodiode

High speed mounted Silicon Photodiode with a spectral response from 350 nm to 1100 nm.

Spectral Response: 350 - 1100 nm

Active Area: 13.0 mm²

Dark Current: 20 nA max. (12 V)

L850P030 Thorlabs Laser Diode

• Wavelength: 850 nm (Typ.)

• Optical Power: 30 mW CW

• Threshold Current: 25 mA (Typ.)

DESCRIPTION	MIN.	TYPICAL	MAX.
Lasing Wavelength (nm)	**840**	**850**	**860**
Threshold Current (mA)	**15**	**25**	**35**
Operating Current (mA)	**40**	**60**	**80**

LT230220P-B Thorlabs 9mm Laser Package Focusing Tube with C230220P-B Optic Pair

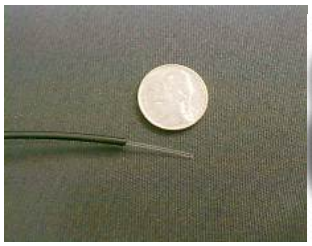

Super ESKA SH4001 Industrial Fibers - Jacketed, plastic optical fiber (1mm)

Fiber Dia. (mm)	Jacket Dia (mm)	Optical Properties			
		Refractive Index		Fiber NA	Acceptance Angle
		Core	Cladding		
1.0	**2.2**	**1.492**	**1.402**	**0.51**	**60**

10610A - SMA 905 Thorlabs Fiber Connectors: Multi-Mode, Fiber Size: 600µm (Ferrule hole size is +10µm over fiber size) Ideal for Large Core Fibers up to 1250µm*SMA style connect*ors are most commonly used with multimode fibers. The ferrule design on the SMA connector makes it an ideal choice for large core fibers. Thorlabs stocks a complete selection of SMA connector sizes to accommodate our full line of large core fibers from 125µm to 1250µm."

Tektronix TDS 1002 Digital Storage Oscilloscope;
60 MHZ, Two channel,

Laser Mounting Tools, Thorlabs

Post

LM1XY/M - Translating Lens Mount: High Resolution Adjuster 250µm/rev. for Sub-micron Sensitivity

PH6-ST Post Holder

S120 Thorlabs Optical Powermeter System
Spectral Range: 400-1100nm
Power Range: 20nW-10mW
Battery operated, optical head has mounting hole to accommodate posts and post holders

LDC500 Thorlabs Laser Diode Driver 500mA

Raytek STPro Noncontact Thermometer
Measures the surface temperature of an object, by sensing emitted, reflected, and transmitted energy, which are collected and focused into a detector.

APPENDIX D
INTRALIPID

Table D.1
Contents of 100 ml intralipid (10%) [27].

Purified soybean oil	10 g
Purified egg phospholipids	1.2 g
Anhydrous glycerol	2.2 g
Water	up to 100 ml of solution

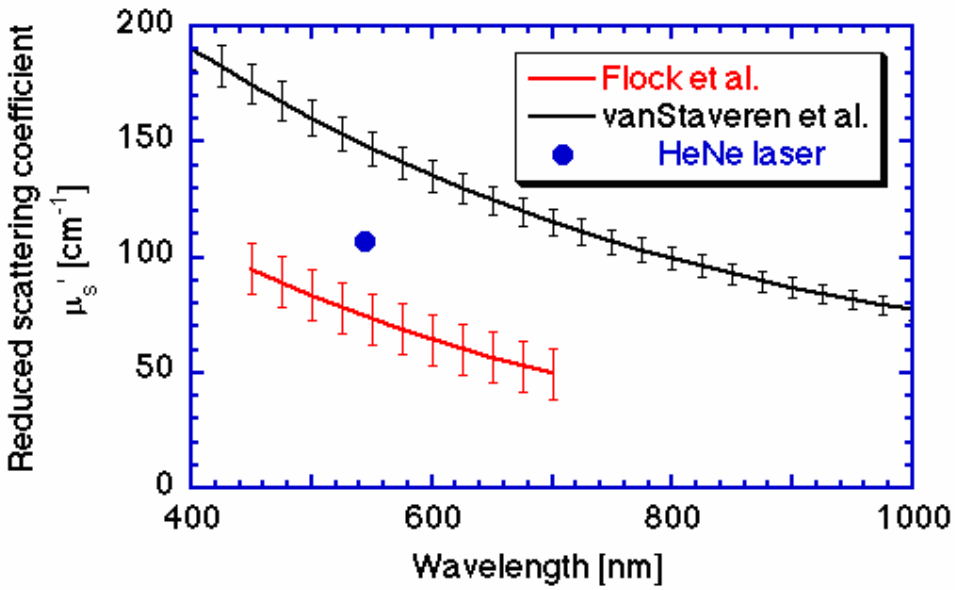

Figure D.1 Reduced scattering constant of intralipid (%10), by three sources [28]

The Mie theory approximation (black line, van Staveren et al.) to μ_s‘ of intralipid (10%) is formulated for wavelengths (nm) [28]:

$$\begin{aligned} mus &= (2.54 \times 10^{9})(nm^{-2.4})\ [cm^{-1}] \\ g &= 1.1 - (0.58 \times 10^{-3})(nm) \\ mus' &= mus(1 - g)\ [cm^{-1}] \end{aligned} \qquad (A.1)$$

APPENDIX E
NOISE SPECTRUM IN FREQUENCY DOMAIN

Fast Fourier Transform (FFT) display of the systems noise is below which is generated by Tektronix TDS 1002 and transferred to computer through WaveStar program. y – axis is the power and each unit stands for 10dB, x – axis is the frequency (Hz) each unit has 1.25 kHz value. We can see our DC signal on the left hand side of the graph at '0 Hz', with a power of 68 dB. The other peaks stand for noise sources at different frequencies. According to FFT transform we observed noise at 2.25 kHz where signal to noise ratio is 30 dB. Also we observed a noise at the same level at 250 Hz at a lower scale (not visible in this figure). In the graph below we also can see noise at frequencies 6.75 kHz and so on that are lower than 50dB of the signal.

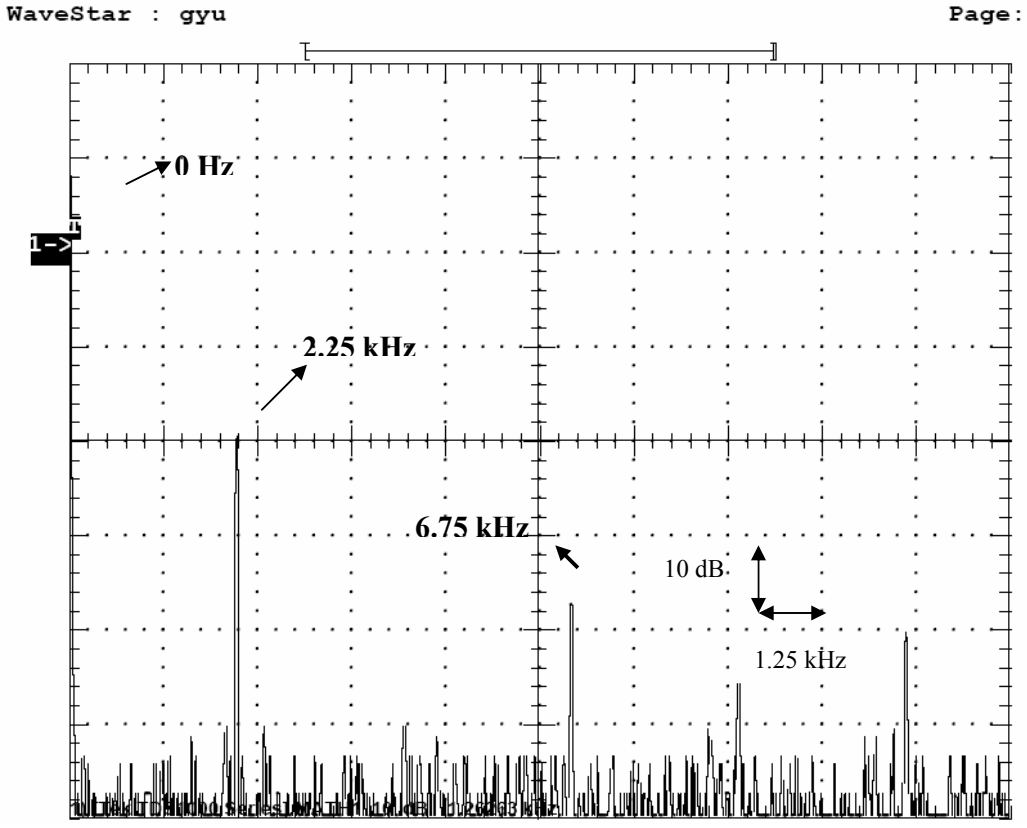

Figure E.1 Fast Fourier Transform of signal observed at the oscilloscope

APPENDIX F
CALIBRATION OF THE SYSTEM

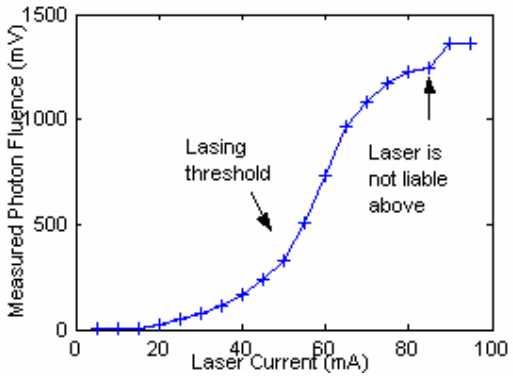

Figure F.1 Output data taken for 0-100 mA using phantom is presented without calibration.

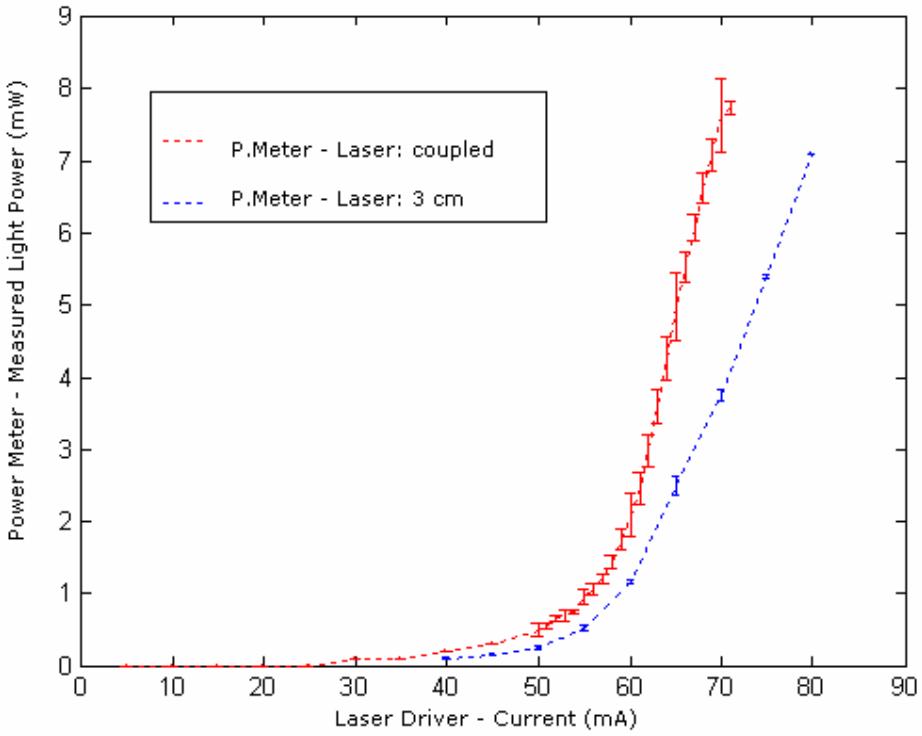

Figure F.2 Diode laser – laser driver characteristics; measured output directly from the collimating tube.

Our first measurements yielded an 'S' curve (Figure F.1). This is due to laser's lasing threshold, max current value and photodiodes characteristics but not due to the phantom. After this measurement lasers output is measured by photodetector (Figure F.2). Red line is the data for detector-laser mount coupled case and the other is for the case that they are 3 cm away. The reason that we took second measurements is that out photodetector is overloaded for an input 850 nm light above 8.2 mW. Our laser gives 8.2 mW output at 70 mA, to see the output for currents above 70 mA is impossible for coupled case, so light is attenuated by keeping tools distant. Results show linearity between 60-80 mA. Our lasers maximum value for input current is 80 mA. Following this to correct the measured data further measurements are done (Figure F.3).

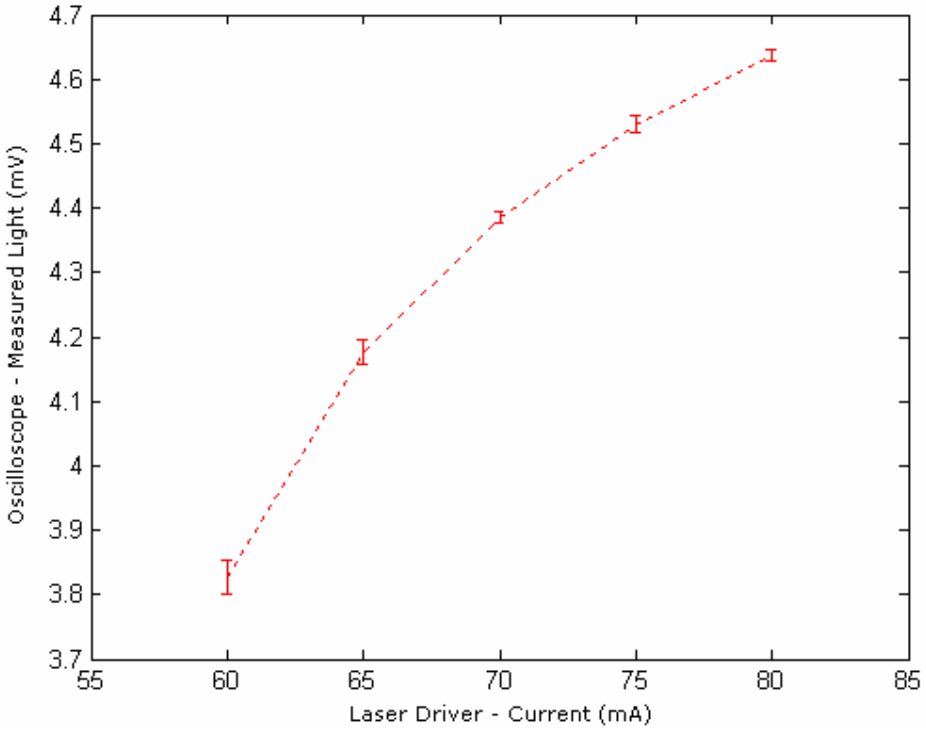

Figure F.3 Light from the input fiber is directly coupled to the photodiode to determine photodiode – amplifier & filter circuit systems effect to the detected signal.

APPENDIX G
DATA

Table G.1
Experimental measurements of output fluence for source – detector (SD) separation 2 cm

Depth of Medium (mm)	SD2 Measurements (mV)			
	At 63 mA	At 65 mA	At 70 mA	At 75 mA
75	670 ±28	755 ±21	900 ±28	995 ±35
15	625 ±35	700 ±28	845 ±21	950 ±28
10	505 ±21	580 ±14	725 ±7.	820 ±14
5	230 ±56	315 ±64	445 ±64	530 ±57

Table G.2
Experimental measurements of output fluence for source – detector (SD) separation 2 cm

Depth of Medium (mm)	SD3 Measurements (mV)			
	At 63 mA	At 65 mA	At 70 mA	At 75 mA
75	375 ±21	465 ±7	610 ±14	695 ±7
15	140	200	320	410 ±14
10	0	45 ±7	170	250
5	0	0	0	25 ±7

Table G.3
PMI data with increase of sensitivity for higher incident light power shown by change of output due to a perturbation layer.

Depth of medium (cm)	SD2 Detected Photon Fluence (joule/cm2) for:		
	1 Watt	3 Watt	5 Watt
4.3	1.3454e-005	4.0362e-005	6.727e-005
4.4	1.3454e-005	4.0363e-005	6.7272e-005
4.5	1.3455e-005	4.0364e-005	6.7273e-005
4.6	1.3455e-005	4.0364e-005	6.7274e-005
4.7	1.3455e-005	4.0365e-005	6.7275e-005
4.8	1.3455e-005	4.0365e-005	6.7275e-005
4.9	1.3455e-005	4.0365e-005	6.7276e-005
5.0	1.3455e-005	4.0366e-005	6.7276e-005
5.1	1.3455e-005	4.0366e-005	6.7276e-005
5.2	1.3455e-005	4.0366e-005	6.7277e-005
5.3	1.3455e-005	4.0366e-005	6.7277e-005
5.4	1.3455e-005	4.0366e-005	6.7277e-005
5.5	1.3455e-005	4.0366e-005	6.7277e-005

APPENDIX H
PROPERTIES OF OPTIC ELEMENTS

H.1 Diode Laser

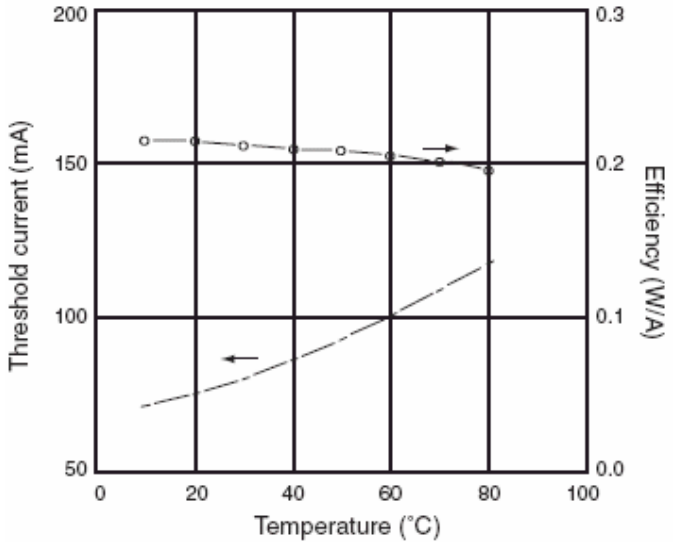

Figure H.1 Threshold current rises and efficiency falls as the temperature increases [29].

There are three essential components to a laser system. First is a *lasing medium*, which may be a gas, crystal, liquid, or semiconductor. Second is a *source of excitation* for the lasing medium, for example, flash lamps or continuous light, radiofrequency, high voltage discharge, diodes, and in some cases another laser. Finally, *mirrors* are needed to reflect the excited photons back into the resonant cavity containing the lasing medium.

As the lasing medium is excited, molecules are "pumped" to a higher energy level. Some of the excited molecules will spontaneously decay to back to the original lower energy, or ground state, releasing a photon, and if the photon is emitted in the right direction, it will hit one of the mirrors at the ends of the resonant cavity and be reflected back into the excited lasing medium. This excited photon can "stimulate" another excited molecule to decay back to the ground state, releasing another photon which travels in the same direction, which in turn is reflected back into the resonant cavity, stimulating emission of even more photons. If most of the molecules in the lasing medium are in the excited state, termed a “population inversion", there is a net amplification of light energy, hence the name *Light Amplification by the Stimulated Emission of Radiation*. Laser light is coherent, collimated and monochromatic as its nature [30].

When an LED-like structure is contained in a resonant cavity formed by polishing the parallel end faces, a diode laser can be formed. A LED is a diode formed form a semicondoctor, such as gallium arsenide (GaAs), that can convert an electrical current into light. The conversion process is fairly efficient in that it generates little heat compared to incandescent lights. Depending on the material, wavelengths (or colors) from the infrared to the near ultraviolet may be produced [32]. Five inherent properties make lasers attractive for use in fiber optics.

1. They are small.
2. They possess high radiance (i.e., they emit lots of light in a small area).
3. The emitting area is small, comparable to the dimensions of optical fibers.
4. They have a very long life, offering high reliability.
5. They can be modulated (turned off and on) at high speeds [31].

H.2 Photodiode

A photodiode is a semiconductor diode that functions as a detector of light. When light with sufficient photon energy strikes a semiconductor junction's depletion region, photons can be absorbed, resulting in generation of a mobile electron and electron hole, these carriers are swept from the junction by the depletion region, producing a current, then light is turned into electric energy.

A p-n junction is formed by combining N-type and P-type semiconductors together in very close contact. The term junction refers to the region where the two types of semiconductor meet. It can be thought of as the border region between the P-type and N-type blocks. Photodiodes are packaged with either a window or optical fibre connection, in order to let in the light to the sensitive part of the device.

A photodiodes sensivity can be increased by enlarging the p-n junction as much as possible. But this results in slowing the response time. Has advantages of:

- Excellent linearity of output current as a function of incident light
- Spectral response from 190 nm to 1100 nm (silicon), longer wavelengths with other semiconductor materials
- Ruggedized to mechanical stress

- Low cost
- Compact and light weight
- Long lifetime
- High quantum efficiency (responsivity), typically 80%

The material used to make a photodiode is critical to defining its properties, because only photons with sufficient energy to excite an electron across the material's bandgap will produce significant photocurrents. Silicon based photodiodes are useful for detection of wavelengths shorter than approximately 1 μm. Germanium photodiodes must be used for wavelengths longer than approximately 1 μm [34].

H.3 Optical Fibers

Optical fibers can be multimode or single mode. The 1.0 mm diameter of the SH4001 is VERY multimode. Optical fibers start to become single mode when their diameter is so small that there is, for all practical purposes, only one path for the light to travel through the core.

Optical fibers are often the device of choice for light delivery to and from a diffusive medium. They can be constructed from a variety of transparent materials. Fibers have a uniform cylindrical core and are surrounded by a cladding made with the same material of a lower refractive index. The difference of refractive indices n_1 and n_2 and that angle of incidence on the core are two factors that total internal reflection depends on. If a light ray strikes the core with an angle that is large enough the condition for internal reflection is violated and the ray escapes through the cladding [27]. So that only a fraction of incident beam coming with an angle below acceptance angle will be collected and transported with continuous reflection all the way through fiber.

APPENDIX I
DICTIONARY

I.1 Necessary Definitions

Various books and sources from the net are used for preparation.

Accuracy: The closeness of a measurement or estimate to its true value

Albedo for single scattering: The probability of a photon surviving an interaction; it equals the ratio of the scattering coefficient to the beam attenuation coefficient.

Coherent: refers to the synchronized phase of the light waves. Imagine 100 soldiers marching in step, and compare to 100 pedestrians at a mall. The soldiers are moving in a coherent manner, compared to the more random motion of the shoppers.

Collimated: refers to the parallel nature of the laser beam. Laser light is emitted in a very thin beam, with all the light rays parallel. By focusing and defocusing this beam, a surgeon can vary its effect on tissue.

Collimating lens: A lens used to collimate light, that is, to gather it together in a parallel beam.

Collimator: A device that filters a stream of photons so that only those travelling parallel to a specified direction are allowed through.

Correlation: Relation between two or more variables.

DOT: The imaging modality that use source and detector arrays, evaluate the incident and measured fluence; with a physical model of light propagation in tissue constructs a 3D map of distribution of the optical scattering coefficient, absorption coefficient, or both, unlike NIRS and gives change of absorption parameters of tissue by time.

Isotropic: Invariant with respect to direction. Isotropic errors have the same statistical distribution in all directions implying equal variance and zero correlation between the original variables (e.g., axis coordinates).

Monochromatic; refers to the single (wavelength) color of a laser beam. Ordinary white light is a mixture of colors, as you can demonstrate by shining sunlight through a prism. Because the wavelength of laser light determines its effect on tissue, the monochromatic property of laser light allows energy to be delivered to specific tissues in specific ways.

Permittivity: Physical quantity that describes how an electric field affects and is affected by a dielectric medium and is determined by the ability of a material to polarize in response to an applied electric field, and thereby to cancel, partially, the field inside the material. Permittivity relates therefore to a material's ability to transmit (or "permit") an electric field

Polydisperse: of, relating to, or characterized by or as particles of varied sizes in the dispersed phase of a disperse system

Precision: The closeness of repeated measurements to the same value

Qualitative: 1. Referring only to the characteristics of something being described, rather than exact numerical measurement. 2. Indicative only of relative sizes or magnitudes, rather than their numerical values. A qualitative comparison would say whether one thing is larger, smaller, or equal to another, without specifying the size of any difference. As opposed to quantitative.

Quantitative: Expressed in numerical values

Resolution: The smallest scale distinguishable by a digitizing, imaging, or display device

Responsivity: The ratio of generated photocurrent to incident light power, typically expressed in A/W when used in photoconductive mode. The responsivity may also be expressed as quantum efficiency or the ratio of the number of photogenerated carriers to incident photons, thus a unitless quantity.

Reverse osmosis: A water treatment process whereby dissolved salts, such as sodium, chloride, calcium carbonate, and calcium sulfate may be separated from water by forcing the water through a semi-permeable membrane under high pressure.

Sandpaper: Zımpara kağıdı.

Sensitivity: For diagnostic tests, the smallest amount of the target molecule that the assay can detect.

Specificity: For diagnostic tests, the ability of a probe to react precisely with a specific target molecule.

I.2 Recommended Nomenclature for Physical Quantities in Medical Applications of Light[3]

I.2.1 Quantities describing the radiation field

Radiant energy *(Q):* Total energy emitted, transferred or received as electromagnetic radiation. The SI unit is J.

Radiant energy flux (Φ): The quotient of *dQ* by *dt,* where *dQ* is the increment of radiant energy in time interval dt. This quantity is identical to the radiant power (see below) and the SI unit is W. While the symbol **Φ** is preferred and is common in the physics literature, its use should be avoided where confusion with quantum yield may arise.

Radiant power (P): Power emitted, transferred or received as electromagnetic radiation. The SI unit is W.

(Energy) fluence *(H_o):* Total radiant energy incident on an infinitesimal sphere containing the point of interest, divided by the cross-sectional area of that sphere. The SI unit is Jm^{-2}.

(Energy) fluence rate *(E_o):* Ratio of total radiant power incident on an infinitesimal sphere containing the point of interest to the cross-sectional area of that sphere. The SI unit is Wm^{-2}. This term is preferable to the equivalent "space irradiance."

[3] AAPM Report [35].

(Energy) radiance *(L):* Radiant energy transported at a given field point in a given direction per unit time per unit solid angle per unit area perpendicular to the propagation direction. The SI unit is W m^{-1} sr^{-1}.

Irradiance *(E):* Radiant power incident on an infinitesimal *surface* element containing the point of interest divided by the area of that element. The SI unit is W m^{-1}. Other terms such as power density, flux density, and intensity which have been used to describe this quantity should be avoided.

Radiant exposure *(H):* Radiant energy incident on an infinitesimal *surface* element containing the point of interest divided by the area of that element. The SI unit is J m^{-2}. The term energy density should be avoided.

Radiant intensity *(I):* Radiant power per unit solid angle. The SI unit is W sr^{-1}.

I.2.2 Quantities describing the interaction of the radiation field with tissue

Index of refraction *(n):* The ratio of the speed of light in vacuum to the speed of light in the medium. Of course tissue is not homogeneous so this can only be defined in the sense of a volume average.

Absorption coefficient *(μ_a):* The probability that a photon will be absorbed on traversing an infinitesimal distance in tissue *(dx),* divided by that distance. In other words, the probability of absorption is $\mu_a dx$.

Scattering coefficient *(μ_s):* The probability that a photon will be scattered on traversing an infinitesimal distance in tissue *(dx),* divided by that distance. The probability of scattering is, therefore, $\mu_s\, dx$.

Total attenuation coefficient *(μ_t):* Sum of the absorption and scattering coefficients. The SI unit is m-1.

Phase function $p(\hat{\Omega},\hat{\Omega}')$ Probability density function describing the angular dependence of scattering. Given that a photon moving in direction $\hat{\Omega}$ is scattered, the probability that it will then be propagating in $d\hat{\Omega}'$ about $\hat{\Omega}'$ is $p(\hat{\Omega},\hat{\Omega}')d\hat{\Omega}'$**.**

Average cosine of scattering angle *(g):* $g = \int_{4\pi} p(\hat{\Omega},\hat{\Omega}')(\hat{\Omega}\bullet\hat{\Omega}')d\hat{\Omega}$. It is usually assumed that tissue is an isotropic medium so that $p(\hat{\Omega},\hat{\Omega}')$ depends only on $(\hat{\Omega}\bullet\hat{\Omega}')$ and g is therefore independent of initial angle.

Mean free path: Mean distance between photon interactions ($1 / \mu_t$). The SI unit is m.

Single scattering albedo *(a):* Ratio of the scattering coefficient to the total attenuation coefficient, $a = \mu_s / \mu_t$.

Transport scattering coefficient *(μ_s'):* The transport or reduced scattering coefficient is given by $\mu_s' = (1\text{-}g)\ \mu_s$ and is an effective isotropic scattering coefficient arising from the diffusion approximation. The SI unit is m^{-1}.

Table I.1
List of physical quantities, symbols, and units [35].

Quantity	**Symbol**	**SI Unit**
Radiant Energy	Q	J
Radiant Energy flux	Φ	W
Radiant Power	P	W
Fluence (Energy)	Ho	J
Fluence rate	Eo	$W\ m^{-2}$
Radiance	L	$W\ m^{-2}\ sr^{-1}$
Irradiance	E	$W\ m^{-2}$
Absorption coefficient	μ_a	m^{-1}
Scattering coefficient	μ_s	m^{-1}
Total attenuation coefficient	μ_t	m^{-1}

APPENDIX J
DATA SHEETS

In the following pages you can find the diagram of the filter and amplifier circuit and data sheets of:

Thorlabs L850P030 Laser Diode

Thorlabs SM05PD1A Photodiode

Eska SH 4001 Optical fiber

Thorlabs S120A Power meter optical head

PHOTODETECTOR CIRCUIT

In the diagram below, R = 1(MΩ), C = 3.3 (nF) and TL071 is used as operational amplifier[4].

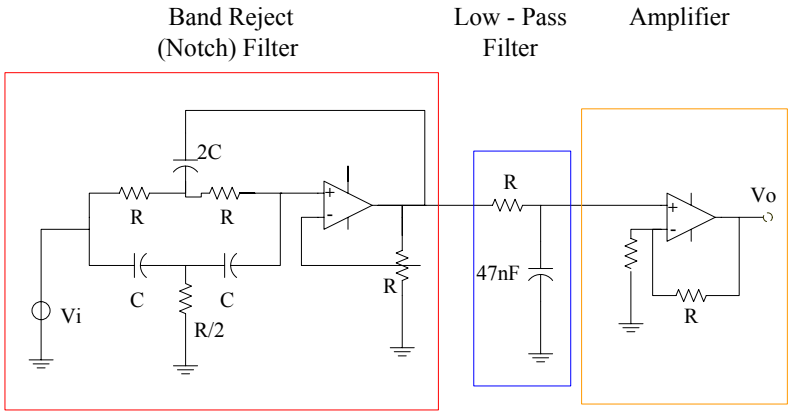

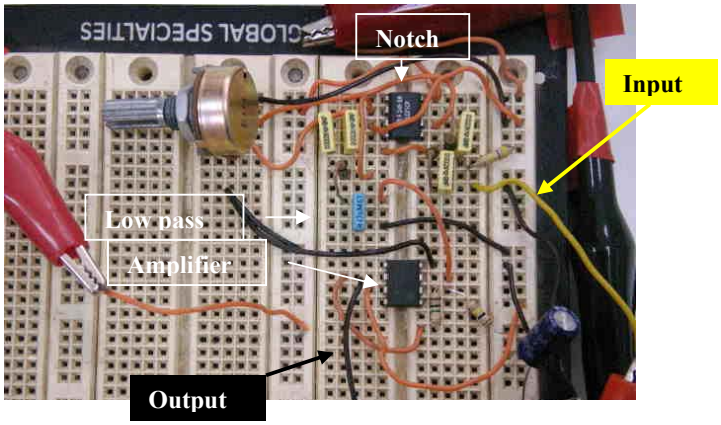

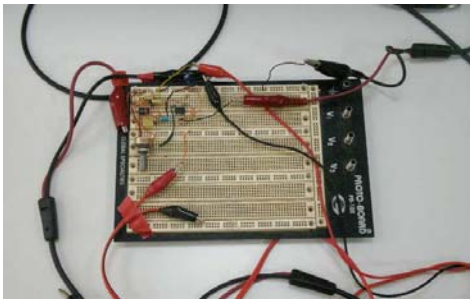

Figure J.1 Photodetector circuit on breadboard (top), with cables (bottom).

[4]Barış Özkerim designed and maintained the circuit for the experiments.

TL071
TL071A - TL071B

LOW NOISE J-FET SINGLE OPERATIONAL AMPLIFIERS

- WIDE COMMON-MODE (UP TO V_{CC}^+) AND DIFFERENTIAL VOLTAGE RANGE
- LOW INPUT BIAS AND OFFSET CURRENT
- LOW NOISE $e_n = 15nV/\sqrt{Hz}$ (typ)
- OUTPUT SHORT-CIRCUIT PROTECTION
- HIGH INPUT IMPEDANCE J-FET INPUT STAGE
- LOW HARMONIC DISTORTION : 0.01% (typ)
- INTERNAL FREQUENCY COMPENSATION
- LATCH UP FREE OPERATION
- HIGH SLEW RATE : 16V/µs (typ)

N
DIP8
(Plastic Package)

D
SO8
(Plastic Micropackage)

DESCRIPTION

The TL071, TL071A and TL071B are high speed J-FET input single operational amplifiers incorporating well matched, high voltage J-FET and bipolar transistors in a monolithic integrated circuit.

The devices feature high slew rates, low input bias and offset currents, and low offset voltage temperature coefficient.

ORDER CODES

Part Number	Temperature Range	Package	
		N	D
TL071M/AM/BM	–55°C, +125°C	•	•
TL071I/AI/BI	–40°C, +105°C	•	•
TL071C/AC/BC	0°C, +70°C	•	•
Example : TL071CN			

PIN CONNECTIONS (top view)

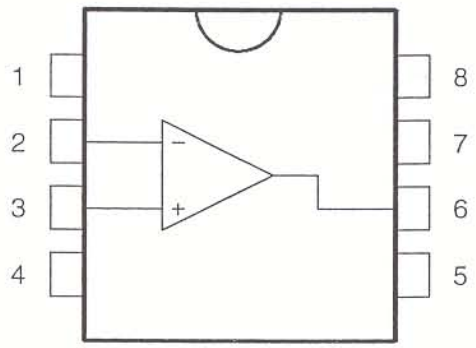

1 - Offset Null 1
2 - Inverting input
3 - Non-inverting input
4 - V_{CC}^-
5 - Offset Null 2
6 - Output
7 - V_{CC}^+
8 - N.C.

THORLABS INC
435 Route 206 • P.O. Box 366
Newton, NJ 07860-0366

SALES 973-579-7227
FAX 973-300-3600

Laser Diode Technical Data

L850P030

Features

- **Index Guided MQW Structure**
- **Wavelength : 850 nm (Typ.)**
- **Optical Power : 30 mW CW**
- **Threshold Current : 25 mA (Typ.)**
- **Package Style : TO-18 (5.6 mmØ)**

ABSOLUTE MAXIMUM RATINGS (Tc=25 °C)

DESCRIPTION	SYMBOL	RATED VALUE
Optical Power (mW)	P_o	**30**
Operation Temperature (°C)	T_{op}	**-10 to +50**
Storage Temperature (°C)	T_{stg}	**-40 to +85**
LD Reverse Voltage (V)	V_{LDR}	**2**
PD Reverse Voltage (V)	V_{PDR}	**30**

OPTICAL AND ELECTRICAL CHARACTERISTICS (Tc=25 °C)

DESCRIPTION	SYMBOL	MIN.	TYPICAL	MAX.	TEST CONDITION
Lasing Wavelength (nm)	λ_p	**840**	**850**	**860**	P_o**=30mW**
Threshold Current (mA)	I_{th}	**15**	**25**	**35**	P_o**=30mW**
Operating Current (mA)	I_{op}	**40**	**60**	**80**	P_o**=30mW**
Operating Voltage (V)	V_{op}	**1.8**	**2.0**	**2.4**	P_o**=30mW**
Monitor Current (mA)	I_m	**0.05**	**0.3**	**1.0**	P_o**=30mW,** V_R**=5V**
Slope Efficiency (mW/mA)	η	**0.3**	**0.5**	**0.7**	***
Beam Divergence ∥ (°)	$\theta\parallel$	**8**	**10**	**12**	P_o**=30mW**
Beam Divergence ⊥ (°)	$\theta\perp$	**25**	**30**	**40**	P_o**=30mW**
Astigmatism (μm)	A_s	*	**11**	*	P_o**=30mW, NA=0.4**

Pin Connection

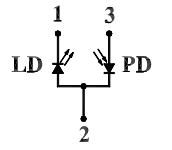

1. Laser diode cathode
2. Laser diode anode
   Photodiode cathode
3. Photodiode anode

* Case and Pin no. 2 are common

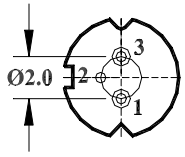

Bottom View

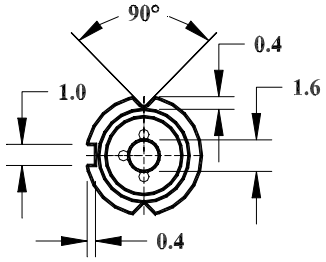

Top View

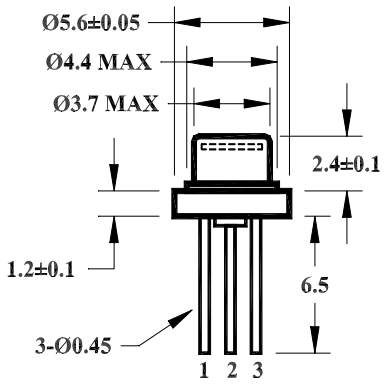

THORLABS INC
435 Route 206 • P.O. Box 366
Newton, NJ 07860-0366
Phone: 973-579-7227
FAX: 973-300-3600

SM05PD1A Mounted Silicon-Photodiode

High Speed
Large Active Area

The SM05PD1A is a high-speed mounted silicon photodiode with a spectral response from 350 nm to 1100 nm. This photodiode has a PIN structure that provides fast Rise/Fall Times (20 ns) with a bias of 12 V. The SM05PD1A is compatible with all Thorlabs SM05 Mounting components.

Electrical Characteristics:

Spectral Response:	350 - 1100 nm
Active Area:	13.0 mm²
Rise Time (R_L = 50 Ω):	20 ns (12 V bias)
Fall Time (R_L = 50 Ω):	20 ns (12 V bias)
NEP @ 900 nm:	1.2 x 10^{-14} $W/\sqrt{Hz}$ (@ 12 V bias)
Dark Current:	20 nA max. (12 V)

Maximum Ratings:

Damage Threshold CW:	100 mW/cm²
Damage 10 ns Pulse:	500 mJ/cm²
Max Bias Voltage:	25 V

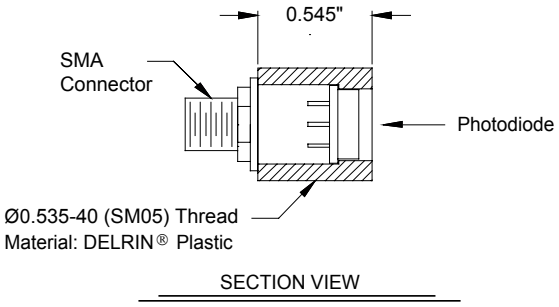

SECTION VIEW

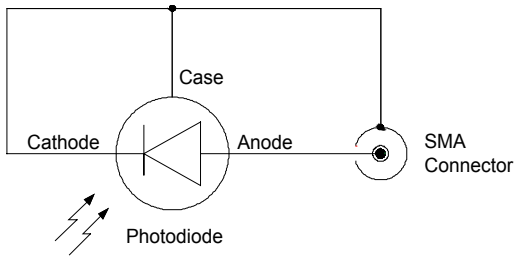

ELECTRICAL CONNECTION

The Thorlabs SM05PD1A Mounted Silicon-Photodiode is ideal for measuring both pulsed and CW light sources, by absorption of photons or charged particles and generate a flow of current in an external circuit, proportional to the incident power. The photodiode anode produces a current, which is a function of the incident light power (P) and the wavelength (λ). The responsivity R_λ, can be read from Fig. 1 to estimate the amount of photocurrent to expect. This can be converted to a voltage by placing a load resistor (R_L) from the photodiode anode to the circuit ground. The output voltage is derived as:

$$V_0 = P \cdot R_\lambda \cdot R_L$$

The bandwidth (f_{BW}) and the rise time response (t_R), are determined from the diode capacitance (C_J) and the load resistance (R_L) as shown below. Placing a bias voltage from the photo diode cathode to the circuit ground can lower the photo diode capacitance.

$$f_{BW} = \frac{1}{2\pi \cdot R_L \cdot C_J} \qquad t_R \cong \frac{0.35}{f_{BW}}$$

Typical Circuit Diagram:

Application of a reverse bias (i.e. cathode positive, anode negative) can greatly improve the speed of response and linearity of the devices. This is due to increase in the depletion region width and consequently decrease in junction capacitance. Applying a reverse bias, however, will increase the dark and noise currents.

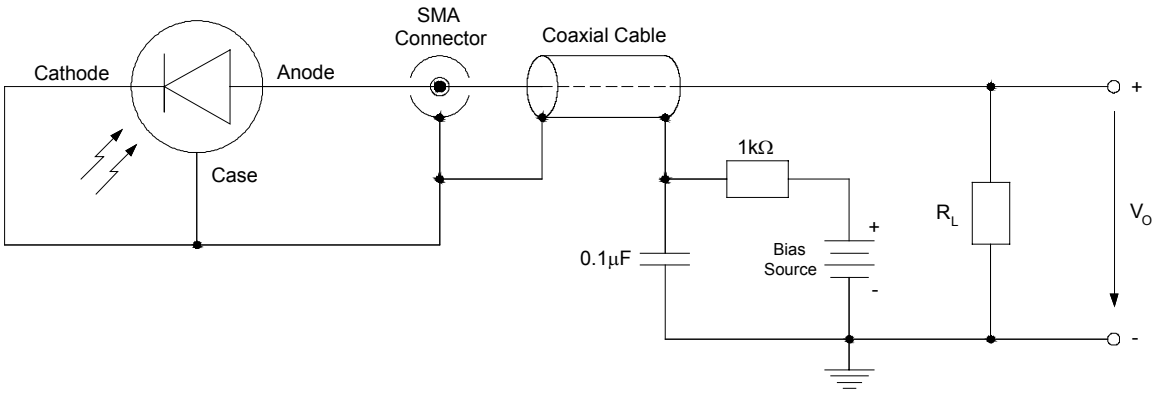

The photodiode output can be either directly connected to an oscilloscope or fed to a fast response amplifier.

Spectral Responsivity:

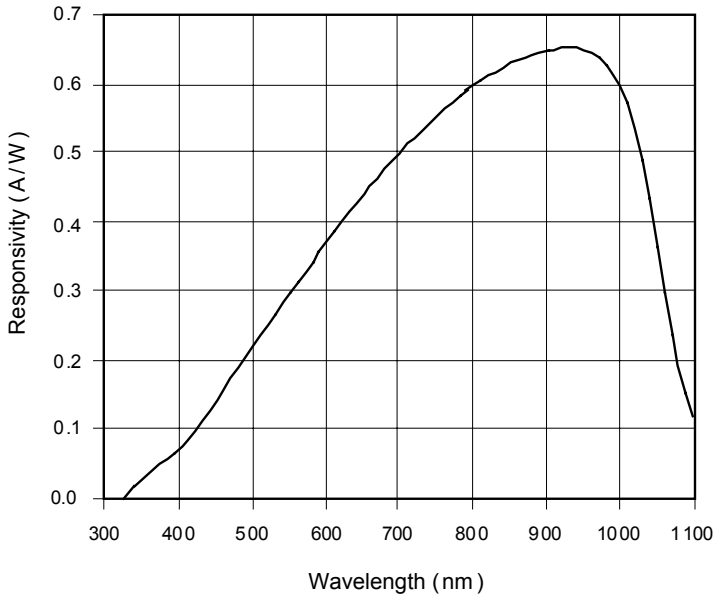

Fig. 1: Spectral Responsivity of SM05PD1A Mounted Si-Photodiode

The responsivity of a photodiode is a measure of the sensitivity to light, and it is defined as the ratio of the photocurrent I_P to the incident light power P at a given wavelength:

$$R_\lambda = \frac{I_P}{P}$$

In other words, it is a measure of the effectiveness of the conversion of the light power into electrical Current. It varies with the wavelength of the incident light as well as applied reverse bias and temperature. Responsivity increases slightly with applied reverse bias due to improved charge collection efficiency in photodiode.

Also there are responsivity variations due to change in temperature, this is due to decrease or increase of the band gap, because of increase or decrease in the temperature respectively. Spectral responsivity may vary from lot to lot and it is dependent on wavelength. However, the relative variations in responsivity can be reduced to less than 1% on a selected basis.

Issued in July , 2001
No. DPF1122-17

Specification Sheet

SH 4001

Super Eska

Polyethylene Jacketed

Optical Fiber Cord

High - Performance Plastic Optical Fiber

Eska™

MITSUBISHI RAYON CO., LTD.
ESKA OPTICAL FIBER DIVISION

6-41 Kounan 1-Chome, Minato-ku, Tokyo, Japan

Phone : + 81 - 3 - 5495 - 3060
Facsimile : + 81 - 3 - 5495 - 3212

No. DPF1122-17

1.Scope

This specification covers basic requirements for the structure, optical and mechanical performances of SH4001.

2.Structure

Table1

Item		SH 4001			
		Specification			
		Unit	Min.	Typ.	Max.
Optical Fiber	Core Material	—	Polymetyl - Methacrylate Resin		
	Cladding Material	—	Fluorinated Polymer		
	Core Refractive Index	—	1.49		
	Refractive Index Profile	—	Step Index		
	Numerical Aperture	—	0.5		
	Core Diameter	μm	920	980	1,040
	Cladding Diameter	μm	940	1,000	1,060
Jacket	Material and Color	—	Polyethylene , Black		
	Diameter	mm	2.13	2.20	2.27
	Indication on the Jacket	—	SUPER ESKA ; Blue		
Approximate Weight		g / m	4		

SUPER ESKA ; Blue

Sectional View

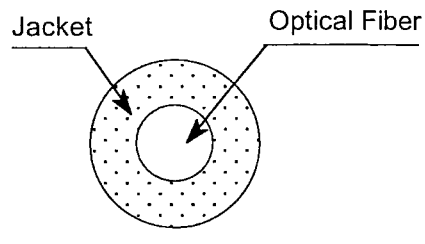

3.Performance

No. DPF1122-17

Table2

Item		Acceptance Criterion and / or [Test Condition]	SH 4001 Specification			
			Unit	Min.	Typ.	Max.
Maximum Rating	Storage Temperature	No Physical Deterioration [in a Dry Atmosphere]	℃	- 55	—	+ 70
	Operation Temperature	No Deterioration in Optical Properties* [in a Dry Atmosphere]	℃	- 55	—	+ 70
	Operation Temperature in a Moist Atmosphere	No Deterioration in Optical Properties** [under 95 %RH]	℃	—	—	+ 60
Optical Properties	Transmission Loss	650 nm Collimated Light]	dB/km	—	—	190
	Transmission Loss under 95 %RH	650 nm Collimated Light]	dB/km	—	—	210
Mechanical Characteristics	Minimum Bend Radius	Loss Increment =< 0.5 dB [A Quarter Bend]	mm	25	—	—
	Repeated Bending Endurance	Loss Increment =< 1 dB [in Conformity to the JIS C 6861]	Times	10,000	—	—
	Tensile Strength	[Tensile Force at 5Åi Elongation; in Conformity to the JIS C 6861]	N	70	—	—
	Twisting Endurance	Loss Increment =< 1 dB [Sample Length : 1 m Tensile Force : 4.9 N]	Times	5	—	—
	Impact Endurance	Loss Increment =< 1 dB [in Conformity to the JIS C 6861]	N.m	0.4	—	—

All tests are carried out under temperature of 25℃ unless otherwise specified.

* Attenuation increase shall be within 10 % after 1,000 hours.
** Attenuation increase shall be within 10 % after 1,000 hours, except that due to absorbed water .

The specification is subject to change without notice.
The information contained herein is presented as a guide for the product selection. Please contact our business department for the issue of an official specification sheet.

Typical Transmission Loss Spectra of POF ESKA™

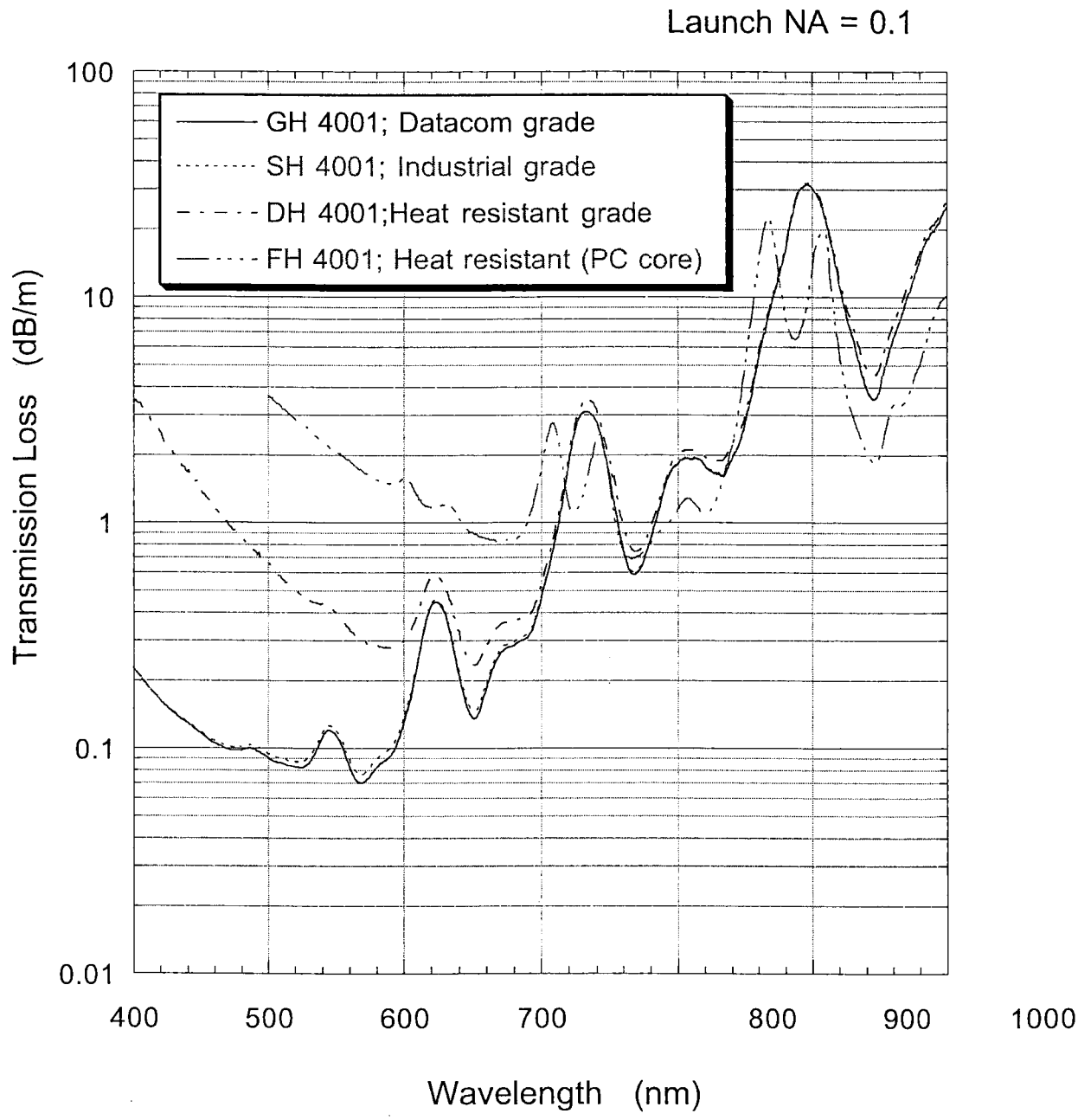

Doc 2614-D04- RevE
02-07-02

Appendix C SPEC SHEET: S120A Silicon Power Meter Optical Head

Description: S120A

The **S120A** is an optical power meter head designed to be used directly with the ThorLabs S110 console system to measure light over the visible wavelength range of 400 to 1100nm and provide a NIST traceable optical power measurement. The optical power meter head will detect light over the power range of 20nW to 10mW. An EPROM located in the DB9 mating connector will store the NIST calibrated spectral response curve required to provide an accurate power reading.

The S120A housing includes a threaded input that is compatible with any number of ThorLabs 1" threaded accessories. This allows convenient mounting of external optics, light filters, and apertures. An 8-32 (M4 for the S120A/M) threaded mounting hole is provided to accommodate posts and post holders.

Mechanical Drawing:

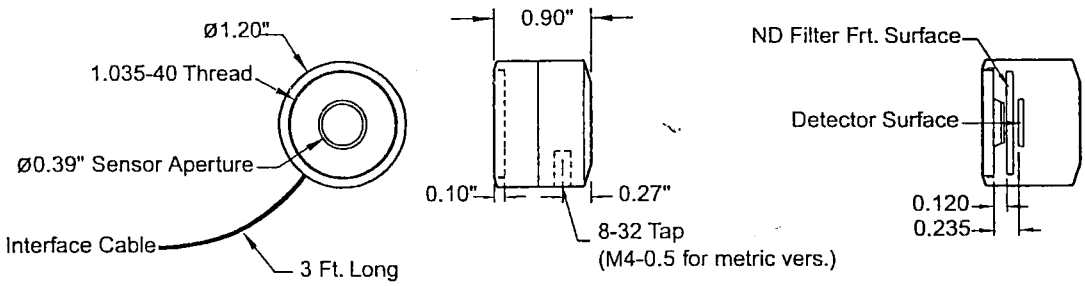

Specifications:

Spectra Range:	400 – 1100nm	Optical Power Range:	20nW – 10mW
Sensor:	Silicon	Resolution:	3.5nW
Sensor Size:	10mm x 10mm sq. (0.39" x 0.39")	Measurement Standard:	NIST Traceable
		Measurement Uncertainty:	+/- 5%
Input Aperture:	0.39" Diameter	Operating Temperature:	5°C to 40°C
Distance to ND Filter:	0.120 inches	Storage Temperature:	5°C to 40°C
Distance to Detector:	0.235 inches		

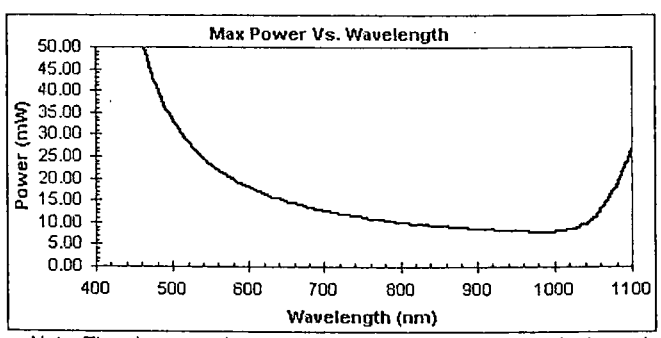

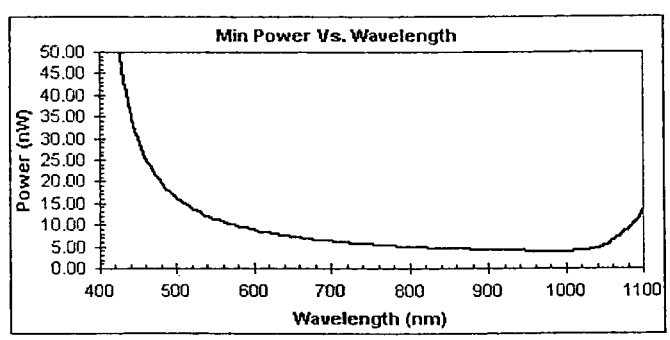

Note: The above graphs are typical values since the power is dependent on the spectral responsivity, which will vary from detector to detector.

Cleaning and Maintenance:

There are no serviceable parts in the S120A optical head. The housing may be cleaned by wiping with a soft damp cloth. When cleaning the aperture filter of the S120A, treat it as any other fine optic. Gently blow off any debris using compressed air and wipe gently with an optic tissue wetted with propanol. If you suspect a problem with your S120A please call ThorLabs and an engineer will be happy to assist you.

As long as the sensor has not been exposed to excessive optical power, the calibration should be very stable over long periods of time (well over a year). However, the detector should be calibrated once a year to ensure accuracy.

REFERENCES

1. Jöbsis, F. F., "Non invasive, infrared monitoring of cerebral and myocardial oxygen sufficiency and circulatory parameters", *Science,* 198 1264 – 7, 1997.

2. Firbank, M., Hiraoka, M, Essenpreis, M. ,Delpy, D. T., "Measurement of the optical properties of the skull in the wavelength range 650 – 950 nm", *Phys Med. Biol*. 38, 1993.

3. Tuchin, V., *Tissue optics.* Bellingham, Wash. SPIE Optical Engineering Press, 2000.

4. A. Siegel, Boas D., *Investigating the Temporal Evolution of the Cerebral Hemodynamic Response Using Diffuse Optical Tomography; Chapter II.* PhD Dissertation, Tufts University, 2004.

5. Elwell, Clare, J. Hebden, "Near – Infrared Spectroscopy", UCL Dept of Medical Physics and BioEngineering – BORL, 1999. Avaliable at: www.medphys.ucl.ac.uk. (Last accessed: 17/6/2006)

6. Boas et al.," Imaging the body with diffuse optical tomography", *IEEE Signal Processing Magazine* IEEE, 2001.

7. Ishimaru, Akira, *Wave propagation and scattering in random media.* Academic Press, 1978.

8. Simon R Arridge, Hebden, J." Optical imaging in medicine: II. Modelling reconstruction", *Phys. Med. Biol.* 42, 1997.

9. Scott, Prahl, *Light transport in tissue*. PhD Dissertation, University of Texas, 1988.

10. O'Leary, M. *Imaging with Diffuse Photon Density Waves*. PhD Dissertation, *Department of Biomedical Optics*, University of Pennsylvania, Philadelphia,1996.

11. Feng S., F. Zeng, B. Chance, "Monte Carlo Simulations of Photon Migration Path Distributions in Multiple Scattering Media", *SPIE* Vol. 1888, 1993.

12. Kumar G., J.M. Schmitt, "Optimal probe geometry for near-infrared spectroscopy of biological tissue", *APPLIED OPTICS* , Vol. 36, No. 10, 1997.

13. Ozer, K. *Optical Properties of native and coagulated lamb brain tissues in vitro in the visible and near – infrared spectral range*. M.S. Thesis, Boğazici University, 2005.

14. PMI Toolbox is a folder of Matlab codes implemented by Boas et al. (Photon Migration Imaging Lab, Harvard University). http://www.nmr.mgh.harvard.edu/~jstott/PMI/. (Last accessed: 17/6/2006)

15. Boas et al., *PMI Toolbox User's Guide*, 2002. Available at: http://www.nmr.mgh.harvard.edu/PMI/resources/toolbox.htm. (Last accessed: 17/6/2006)

16. Boas, D. A., Gaudatte, T., Arridge, S., "Simultaneous imaging and optode calibration with diffuse optical tomography", *OPTICS EXPRESS*, Vol. 8, No. 5, 2001.

17. M. Woodward, "A qualitative comparison of the first order Born and Rytov approximations", *SEP*, 60, 1989.

18. Yoo, K.M., Liu, Feng and R. R. Alfano," When does the diffusion approximation fail to describe photon transport in random media?**"** *Phys. Rev. Lett.* 64, 2647–2650,1990.

19. *LDC 500 Laser Diode Controller Instruction Manual* Thorlabs, Inc. 2000.

20. Nick, Bertone, Webb P., "Noise and Stability in PIN Detectors", PerkinElmer Optoelectronics, 2003. http://optoelectronics.perkinelmer.com/content/whitepapers/NoiseandStabilityPINDetectors.pdf

21. Steen J Madsen, Patterson M., Wilson B., "The use of Indian ink as an optical absorber in tissue-simulating phantoms", *Phys. Med. Biol.,* Vol. 31, No 4, 1992.

22. Flock ST, Jacques SL, Wilson BC, Star WM, van Gemert MJ,"Optical properties of Intralipid: a phantom medium for light propagation studies." *Lasers Surg Med.;*12(5):510-9, 1992.

23. HG van Staveren, CJM Moes, J van Marle, SA, Prahl, MJC van Gemert, "Light scattering in Intralipid-10% in the wavelength range of 400-1100 nanometers," *Applied Optics* 30:4507-4514, 1991.

24. S. Jacques, "Optical properties of "Intralipid^{TM}", an aqueous suspension of lipid droplets", Oregon Medical Laser Center, 1998. Available at: http://omlc.ogi.edu/spectra/intralipid/index.html. (Last accessed: 17/6/2006)

25. Boas, D. "Diffuse Photon Probes of Structural and Dynamical Properties of Turbid Media: Theory and Biomedical Applications-Chapter 7", PhD Dissertation, University of Pennsylvania 1996.

26. Borl Research Activity – University Collage London, Biomedical Optics Research Laboratory. Available at: http://www.medphys.ucl.ac.uk/research/borg/research.htm

27. Valery V., Tuchin*, Handbook of optical biomedical diagnostics*, SPIE Press, 2002.

28. Optical properties of intalipid – http://omlc.ogi.edu/spectra/intralipid/index.html.(Last accessed: 17/6/2006)

29. Tyll Hertsens, "Measuring Diode Laser Characteristics" http://www.ilxlightwave.com/appnotes/overview_laser_diode_characteristics.pdf. (Last accessed: 17/6/2006)

30. More about Lasers – http://www.shorelaser.com/AboutLasersDet.html. (Last accessed: 17/6/2006)

31. Laser Diode – http://www.fiber-optics.info/articles/laser-diode.htm.(Last accessed: 17/6/2006)

32. Laser Diode – http://en.wikipedia.org/. (Last accessed: 17/6/2006)

33. COMLAB – www.e-prolab.com/comlab/sttop/sttopoe/CHAPTER3/. (Last accessed: 17/6/2006)

34. ATIS Telecom Glossary, 2000. http://www.atis.org/tg2k/t1g2k.html. (Last accessed: 17/6/2006)

35. American Association of Physicists in Medicine (AAPM), General Medical Physics Committee, "AAPM Report No. 57, Recommended Nomenclature for Physical Quantities in Medical Applications of Light", American Institute of Physics, 1996. Available at; www.aapm.org/pubs/reports/rpt_57. (Last accessed: 17/6/2006)

36. Ntziachristos V.,Chance B., "Breast imaging technology: Probing physiology and molecular function using optical imaging - applications to breast cancer "-Review- *Breast Cancer Res* 3:41-46, 2001.

37. Hillman, E., Boas D.A.,"Laminar optical tomography: demonstration of millimeter-scale depth-resolved imaging in turbid media", *OPTICS LETTERS* / Vol. 29, No.14 (2004)

38. Sakudo et al.," Near-infrared spectroscopy: Promising diagnostic tool for viral infections", *Biochemical and Biophysical Research Communications* 341 279–28, 2006.

39. Yodh, G., Boas D. A., *Biomedical Photonics Handbook; Chapter 21: Functional imaging with diffusing light*. CRC Press, 2002.

40. M. Canpolat, Mourant J. R.," Particle size analysis of turbid media with a single optical fiber in contact with the medium to deliver and detect white light", Applied Optics, Vol. 40, No. 22, 2001.

41. F., Zhang et al.," Non invasive determination of tissue optical properties based on radiative transfer theory", *Optics & Laser Technology*, 2003.

42. Walker, S.A., D., Boas,"Photon density waves scattered from cylindrical inhomogeneities", *Applied Optics,* 37-10, 1998.

43. Aydin, E. D., C. R., Oliveira, A., Goddard "A comparison between transport and diffusion calculations using a finite element-spherical harmonics radiation transport method", Med. Phys. 29-9, 2002.

44. Gaudette, Rick *Constrained Reconstruction Techniques for Diffuse Optical Tomography,* PhD Dissertation. Tufts University, 2000.

45. Elwell, C., "Shedding light on the brain", *NIR News* Vol. 16 No. 7, 2005.

46. Fidan, M., *Modeling of photon migration in tissue*, M.S. Thesis. Boğaziçi University, 2005.

47. Gibson, Hebden, J., Arridge, S. "Recent advances in diffuse optical imaging", *Phys. Med. Biol.* 50, 2005.

48. Rebecca Richards-Kortum, Muraca, E.,"Quantitative optical spectroscopy for tissue diagnosis", *Annu. Rev. Phys. Chem.,* 47, 1996.

49. Jorge Ripoll, Lorenzo, *Light diffusion in turbid media with biomedical application*, PhD Dissertation. Universidad Autonoma de Madrid, 2000.

50. FDA, Office of Science and Technology - Annual Report - Fiscal Year 1997 Avaliable at http://www.fda.gov/cdrh/ost/rpt97/ (Last accessed: 17/6/2006)